

Science Opportunities of Wet Extreme Mass-Ratio Inspirals

Zhenwei Lyu,^{1,*} Zhen Pan,^{2,3} Junjie Mao,⁴ Ning Jiang,^{5,6} and Huan Yang^{4,†}

¹*Leicester International Institute, Dalian University of Technology, Panjin 124221, China*

²*Tsung-Dao Lee Institute, Shanghai Jiao-Tong University, Shanghai, 520 Shengrong Road, 201210, China*

³*School of Physics & Astronomy, Shanghai Jiao-Tong University, Shanghai, 800 Dongchuan Road, 200240, China*

⁴*Tsinghua University, Department of Astronomy, Beijing 100084, China*

⁵*CAS Key Laboratory for Research in Galaxies and Cosmology, Department of Astronomy, University of Science and Technology of China, Hefei 230026, People's Republic of China*

⁶*School of Astronomy and Space Sciences, University of Science and Technology of China, Hefei 230026, People's Republic of China*

Wet extreme mass-ratio inspirals (wet EMRIs), which arise from stellar-mass black holes (sBHs) inspiral into supermassive black holes (SMBHs) within the gas-rich environments of Active Galactic Nuclei (AGN), are primary sources of gravitational waves (GWs) for space-borne detectors like LISA, TianQin, and Taiji. Unlike “dry EMRIs”, which form through gravitational scattering in nuclear star clusters, wet EMRIs are naturally accompanied by interactions with accretion disks, offering rich multi-messenger science opportunities. They are distinct in generating transient electromagnetic (EM) signals, such as quasi-periodic eruptions (QPEs), which serve as valuable probes of accretion disk physics and SMBH environments. Their GW signals provide an unprecedented precision of the order of $O(10^{-4} \sim 10^{-6})$ in measuring SMBH mass and spin, enabling the calibration of traditional EM techniques and offering insights into jet formation models. Additionally, wet EMRIs serve as bright and dark sirens for cosmology, facilitating percent-level precision measurements of Hubble parameter through AGN host identification or statistical association. These systems hold immense potential for advancing our understanding of black hole dynamics, accretion physics, and cosmology.

I. INTRODUCTION

Extreme mass-ratio inspirals (EMRIs) and massive black hole (BH) binaries are the two main extragalactic sources of space-borne gravitational wave detectors, such as LISA (Laser Interferometer Space Antenna) [1–4], Tianqin [5–8] and Taiji [8–10], which operate in the millihertz frequency band. In particular, EMRIs are known for their superior precision in measuring weak environmental forces, including tidal gravitational forces from nearby stellar-mass objects [11], disk forces associated with Active Galactic Nuclei (AGN) [12–16], and dynamical friction from clouds of Axion-like particles populated around massive BHs [17–20].

Those EMRIs formed through the interaction with accretion disks are often referred as “Wet EMRIs” [21]. It was previously pointed out in [22] that star formation and evolution within AGN may lead to this class of objects. More recently, quantitative modeling of the nuclear star cluster and the accretion disk have shown that disk capture and migration of a stellar mass object may also give rise to rapid formation of wet EMRIs that eventually merge with the central massive BHs [21]. Based on a class of the disk and cluster models, the inferred rate is comparable to or larger than those EMRIs formed through gravitational scattering within the nuclear cluster (the “Dry EMRIs”) [23, 24].

In this work, we discuss several science opportunities associated with wet EMRIs. First, we propose the existence of a class of X-ray transients broadly connected to the observed quasi-periodic eruptions (QPEs [25–34]). If the accretion disk is inclined with respect to the spin direction of the massive BH, a stellar-mass black hole (sBH) initially migration within

the disk at larger radii may exit the warped accretion disk at a smaller distance, where the GW backreaction dominates the orbital evolution. The sBH may collide with the warped disk twice per orbit, with ejected gas forming expanding fireballs that emit X-rays. This suggests that there is possibly a class of QPE-like transients without the association of Tidal Disruption Events (TDEs), which we refer as type II QPEs.

Second, we point out two promising applications of multi-messenger observation (GWs and the AGN) of wet EMRIs. It turns out that to locate wet EMRIs in their host galaxy, the LISA sensitivity limits the source redshift to ≤ 0.3 . For these wet EMRIs, the measurement precision of mass and spin is generally on the order of $O(10^{-4} \sim 10^{-6})$ [2], which may serve as an accurate calibration tool for other methods of measuring BH mass and spin, such as using the broad line $H\beta$ or the X-ray spectrum. In particular, to calibrate the X-ray measurement for BH spins, we find that only sources with redshift ≤ 0.1 may have enough X-ray luminosities detectable by flagship missions such as Athena and eXTP. On the other hand, as GW observations can be used to measure the direction of massive BH spin, the inclination of the sBH may be used to constrain the normal direction of the accretion disk. If there is radio observation of a possible jet associated with the AGN, this multi-messenger measurement of the BH spin, jet, and disk inclination may be used to test jet formation models.

Third, wet EMRIs offer new opportunities to study cosmology. Since we expect that wet EMRIs are associated with AGNs, searching for candidates for AGN within the error volume determined by GW measurements greatly reduces the number of candidates for wet EMRIs. This advantage applies for both bright sirens with nearby wet EMRIs (with host galaxy identification available) and dark sirens for more distant wet EMRIs. Both methods are expected to produce percent-level-precision measurement on the Hubble parameter with one-year observation of LISA. Taking into account

* zwlyu@dlut.edu.cn

† hyangdoa@tsinghua.edu.cn

the possibility that only a fraction of AGN is observed, e.g. due to dust attenuation, does not significantly change this estimate.

These topics are by no means an exclusive list of astrophysical and cosmological applications of wet EMRIs. For example, if the surface density of the disk is sufficiently high at $O(10)$ gravitational radii [12, 13] and/or the orbital eccentricity is significant [16], the disk effect imprinted on the gravitational waveform may be detectable. Wet EMRIs may also be used to probe intermediate-mass BHs that are captured in the accretion disk [35], as these less massive objects may form mean-motion resonance pairs or chains within the AGN disk [36]. In addition, the population of unresolved wet EMRIs may give rise to a stochastic GW background that is observable by space-borne GW detectors [37]. The scientific opportunities discussed in this work are complementary to these previous studies, which we hope will motivate further exploration in this direction.

The structure of this work is organized as follows. In Sec. II A, we discuss the formation and population of wet EMRIs, including their formation mechanisms in accretion disks and population estimates based on updated SMBH mass functions. In Sec. II B, we explore transient electromagnetic (EM) counterparts, focusing on the connection between wet EMRIs and QPEs. In Sec. II C, we address how wet EMRIs can be used to calibrate other methods of probing BH mass and spin. In Sec. II D, we examine the potential of wet EMRIs to test accretion disk and jet models. Finally, in Sec. II E, we discuss the application of wet EMRIs as cosmic sirens. Resolvable host AGNs enable their use as bright sirens (yielding luminosity distance and redshift), while unresolvable hosts result in dark sirens. Finally, in Sec. III, we discuss possible uncertainties and caveats in this analysis, and motivate further studies in this emerging field.

II. MULTI-MESSENGER SCIENCE OPPORTUNITIES

A. Population estimation

For sBHs on inclined and/or eccentric orbits, strong interactions with the accretion disk of a rapidly accreting SMBH play a crucial role in their evolution. These interactions, mediated by dynamical friction and disk-induced density waves, damp the orbital inclination and eccentricity of the sBH relative to the disk plane and eventually capture the sBH into the disk. Once captured, the sBH begins to migrate inward, driven by the density waves it excites through its periodic motion within the disk.

For lower-mass sBHs, type-I migration dominates, where the sBH interacts with the surrounding disk material, resulting in continuous inward drift. The timescale for type-I migration is given by [38, 39]

$$t_{\text{mig,I}} \sim \frac{M}{\mu} \frac{M}{\Sigma} \frac{h^2}{r^2 \omega_K}, \quad (1)$$

where $M = M(< r)$ is the total mass enclosed within the orbital radius r , μ is the sBH mass, $\Sigma(r)$ is the disk surface den-

sity, $h(r) = H(r)/r$ is the disk aspect ratio (with H being the characteristic vertical thickness of the disk at a given radius r from the central object), and ω_K is the Kepler angular velocity. For more massive sBHs capable of opening a gap in the accretion disk, type II migration takes over. In this case, the migration is slower and is governed by the viscous evolution of the disk itself.

The structure and dynamics of the accretion disk also influence the migration and formation rates of EMRIs. In α -type disks, the viscosity scales with the total pressure (which includes both the gas and radiation pressure), while in β -type disks the viscosity scales with the surface density of the disk. These differences affect the disk's structure and, consequently, the migration timescales and efficiency. Migration continues until the sBH approaches the SMBH, where GW emission dominates, driving the final inspiral. The presence of accretion flows accelerates both the capture of sBHs into the disk and their inward migration, significantly increasing the EMRI formation rate compared to the dry channel, where no disk is present [23].

The formation and population of wet EMRIs depend on several factors, including the fraction of SMBHs hosted in AGNs, the structure of the accretion disk, and the initial distribution of sBHs in the surrounding stellar cluster. Observational studies suggest that approximately 1% \sim 10% of the SMBHs reside in AGNs, the fraction varying by redshift. For simplicity, we conservatively assume a constant AGN fraction of $f_{\text{AGN}} = 1\%$ throughout the universe.

The SMBH mass function is critical to estimate the wet EMRI population. Two representative SMBH mass functions are commonly used:

1. Population III seeded Model [40–42]

$$\frac{dN_{\bullet}}{d \log M_{\bullet}} = 0.01 \left(\frac{M_{\bullet}}{3 \times 10^6 M_{\odot}} \right)^{-0.3} \text{Mpc}^{-3},$$

2. Phenomenological Model [43]

$$\frac{dN_{\bullet}}{d \log M_{\bullet}} = 0.002 \left(\frac{M_{\bullet}}{3 \times 10^6 M_{\odot}} \right)^{+0.3} \text{Mpc}^{-3}.$$

In both cases, $dN_{\bullet}/d \log M_{\bullet}$ represents the number density of SMBHs per logarithmic mass interval. These mass functions were used in our previous studies [21, 23] to estimate the abundance of SMBHs in the range $10^4 \sim 10^7 M_{\odot}$, which is particularly relevant for the formation and detection of EMRI. Our results demonstrated that wet EMRI could significantly enhance total and detectable EMRI rates, often dominating over dry EMRI.

Recent studies based on optical observations of TDEs have provided an updated local SMBH mass function, which is nearly flat in logarithmic space [44], given by

$$\frac{dN_{\bullet}}{d \log M_{\bullet}} = 0.005 \left(\frac{M_{\bullet}}{3 \times 10^6 M_{\odot}} \right)^{\beta} \text{Mpc}^{-3}, \quad (2)$$

TABLE I. Forecasted rates for stellar-mass black hole (sBH) EMRIs in the redshift range $0 < z < 4.5$, with the mass of sBH $\mu = 10M_\odot$. The table presents total EMRI rates, LISA detection rates (with $\text{SNR} \geq 20$) and rates for which the host AGN galaxy is resolvable. Wet EMRI models follow the configuration of our previous work [21, 23], assuming a conservative AGN fraction $f_{\text{AGN}} = 1\%$ throughout the universe. For comparison, the last row shows dry EMRI rates with $N_p = 10$ plunges per EMRI.

Wet EMRIs	AGN disk	T_{disk} [yr]	Total rates [yr^{-1}]	detection rates [yr^{-1}]	resolvable hosts [yr^{-1}]
	α -disk	10^6	2700	120	30
		10^7	1100	40	9
		10^8	390	13	3
	β -disk	10^6	3500	150	32
		10^7	1200	50	10
		10^8	390	13	3
Dry EMRIs	N_p		Total rates [yr^{-1}]	detectable rates [yr^{-1}]	
	10		480	45	-

with a power index $\beta \approx 0$. This updated mass function offers a more accurate description of SMBHs in the mass range $10^4 \sim 10^7$, which is critical for EMRI formation. Unlike earlier models that extrapolated SMBH populations from higher masses ($\sim 10^7 M_\odot$) [2], the TDE-based estimates are directly informed by observations of SMBHs with masses as low as $10^5 M_\odot$ [44].

With this updated mass function, we have reevaluated the population and detection rates of wet EMRIs, as summarized in Table I. The total wet EMRI rate across all SMBHs is calculated by integrating the differential EMRI rate over the mass M_\bullet and redshift z . The differential rate is given by

$$\frac{d^2 \mathcal{R}_{\text{wet}}}{dM_\bullet dz} = \frac{f_{\text{AGN}}}{1+z} \frac{dN_\bullet}{dM_\bullet} \frac{dV_c(z)}{dz} C_{\text{cusp}}(M_\bullet, z) \Gamma_{\text{wet}}(M_\bullet), \quad (3)$$

where the factor $1/(1+z)$ arises from the cosmological redshift, $V_c(z)$ is the comoving volume of the universe up to redshift z , $C_{\text{cusp}}(M_\bullet, z)$ is the fraction of SMBHs living in stellar cusps [45]. The time-averaged wet EMRI rate per AGN, $\Gamma_{\text{wet}}(M_\bullet)$, depends on the disk lifetime T_{disk} , the rate of sBH capture, and the migration timescale [21, 23, 24].

Table I summarizes the updated wet EMRI population estimates based on the revised SMBH mass function. The table provides the total wet EMRI rates for sBHs ($\mu = 10M_\odot$) over the redshift range $0 < z < 4.5$, as well as the corresponding LISA detection rates (for a signal-to-noise ratio $\text{SNR} \geq 20$) and the fraction of resolvable host AGN galaxies. A host galaxy is considered resolvable if the expected number of AGNs within the localization volume is less than 1.1 (as detailed in Sec. II E). These calculations are based on the framework established in our previous work [21, 23], assuming a conservative AGN fraction of $f_{\text{AGN}} = 1\%$ throughout the universe. For comparison, the final row includes the dry EMRI rates, assuming $N_p = 10$, where N_p represents the number of plunges per EMRI.

To access the LISA detection rates, we adopt the Augmented Analytic Kludge (AAK) waveform model [46, 47], which has been implemented in FEW [47–49]). These waveforms are generated for the last two years of inspiral before coalescence and are expressed in the time domain for both GW polarizations. The LISA detector's response to these wave-

forms is modeled using its two orthogonal channels (I and II), with the GW signals projected as [50, 51]

$$h_I(t) = h_+(t) F_I^+(t) + h_\times(t) F_I^\times(t), \quad (4)$$

$$h_{II}(t) = h_+(t) F_{II}^+(t) + h_\times(t) F_{II}^\times(t), \quad (5)$$

where $h_+(t)$ and $h_\times(t)$ are the two GW polarizations, and $F_I^+(t)$, $F_I^\times(t)$, $F_{II}^+(t)$, and $F_{II}^\times(t)$ are the antenna pattern functions of the LISA detector for each channel. The SNR used to assess the detectability of EMRIs is defined as

$$\rho = \sqrt{\langle h_I | h_I \rangle + \langle h_{II} | h_{II} \rangle}, \quad (6)$$

where the inner product is given by

$$\langle a, b \rangle = 4 \text{Re} \int_{f_{\text{min}}}^{f_{\text{max}}} \frac{\tilde{a}(f) \tilde{b}^*(f)}{P_n(f)} df. \quad (7)$$

where $\tilde{a}(f)$ and $\tilde{b}(f)$ are the Fourier transforms of the signals $a(t)$ and $b(t)$, and $P_n(f)$ represents the one-sided spectral noise density of the LISA detector [1, 52, 53]. The detection threshold is set at $\rho = 20$ [2]. The corresponding LISA detection rates are listed in the second-to-last column of Table I.

The inclusion of the TDE-based SMBH mass function enhances our ability to model wet EMRI populations and their detectability, providing a refined picture of their contribution to the GW event rate.

B. Transient Electromagnetic Counterparts: type II QPEs

In a gas-rich environment, it is natural to expect EM emissions as the sBH travels through the gas around the SMBH. If the sBH is aligned with and embedded in the gas disk, the continuous EM emission arising from gas accretion into the sBH will be reprocessed by the disk and will be hard to distinguish from the AGN background emission. In this case, the environmental effects on the gravitational waveform of EMRI have been investigated in previous studies [12–16]. Notice that the disk orientation at larger radii may not be the same as the local disk direction, where the local disk is likely perpendicular to the SMBH spin direction [54], while the outer

disk direction depends on the angular momentum of the gas feeding at larger radii. The wrapped disk will exert a torque onto the central BH and align or antialign the BH spin with the angular momentum of the outer disk. The wrap radius is approximately [55, 56]

$$\frac{R_{\text{wrap}}}{M_{\bullet}} \approx 12 \left(\frac{\alpha}{0.1} \right)^{2/3} a^{2/3} \left(\frac{h}{0.1} \right)^{-4/3}, \quad (8)$$

and the disk alignment timescale in the small wrap case is approximately [55–59]

$$t_{\text{align}} \approx 1.2 \times 10^6 \text{ yr} \left(\frac{\dot{M}_{\bullet}}{\dot{M}_{\bullet, \text{Edd}}} \right)^{-1} \left(\frac{\alpha}{0.1} \right)^{5/3} a^{2/3} \left(\frac{h}{0.1} \right)^{2/3}, \quad (9)$$

where α is the standard viscosity coefficient in thin disks, a is the dimensionless spin of the SMBH, \dot{M}_{\bullet} is the SMBH accretion rate and the Eddington accretion rate $\dot{M}_{\bullet, \text{Edd}} = \dot{M}_{\bullet}/(5 \times 10^7 \text{ yr})$, and h is the disk aspect ratio. If the accretion of the SMBH is coherent in a period much longer than t_{align} , we expect an equatorial accretion disk and an equatorial EMRI when the EMRI enters the LISA band; therefore, no detectable EM transient is produced. Otherwise, if the gas feeding direction is random in each accretion episode with an accretion time scale shorter than t_{align} , EM transients arising from EMRI and disk collisions are possible: for a sBH embedded in the disk, the Lense-Thirring precession tends to drive its orbit out of the disk plane, while the disk interaction tends to keep the sBH within the plane. We denote the critical radius as r_{dec} where the alignment timescale for the sBH orbit with the disk is equal to the Lense-Thirring precession timescale of the sBH. At smaller radii $r < r_{\text{dec}}$, the sBH orbiting around the SMBH may hit the accretion disk and produce (quasi-)periodic EM transients, similar to some of the discussion of X-ray quasi-periodic eruptions (QPEs) [25–34], where eruptions are highly likely due to collisions between a low-frequency ($f_{\text{obt}} \sim 10^{-5}$ Hz) EMRI and an accretion disk formed in a recent TDE [33, 34, 60–70]. For clarity, we will call the TDE-associated QPEs as type I QPEs and the quasi-periodic EM transients produced by an EMRI crossing an AGN disk as type II QPEs:

- Type I QPE: QPE associated with a TDE
- Type II QPE: QPE associated with an AGN and without a TDE

Notice that Swift J023017 is likely a type II QPE source as analyzed in [66], which is associated with a low luminosity AGN.

In the remainder of this section, we first estimate the decoupling radius r_{dec} of wet EMRIs, then the energy budget of type II QPEs and finally evaluate the possibility for multi-messenger detections of wet EMRIs in the LISA era. Considering a sBH embedded in an accretion disk which is misaligned with the SMBH equator, the Lense-Thirring precession tends to drive the sBH out of the disk plane in a rate

$$\vec{\omega}_{\text{LT}} = \frac{2\vec{a}}{r^3}, \quad (10)$$

where \vec{a} is the dimensionless spin vector of the central SMBH and r is the orbital radius. The disk interaction tends to align the secondary massive object (SMO) orbital plane with the disk plane at a rate $\vec{\omega}_{\text{DI}}$ (in the direction of $\vec{n}_{\text{disk}} \times \vec{L}$), where \vec{n}_{disk} is the normal vector of the disk and \vec{L} is the angular momentum of the SMO orbit. The orbital angular momentum \vec{L} evolves according to

$$\frac{d\vec{L}}{dt} = (\vec{\omega}_{\text{LT}} + \vec{\omega}_{\text{DI}}) \times \vec{L}, \quad (11)$$

Denoting the inclination of the sBH orbit relative to the disk as t_{sd} , the alignment is driven by dynamical friction at large inclinations and by density waves at small inclinations [71, 72], with a rate

$$\omega_{\text{DI}} := -\frac{dt_{\text{sd}}}{dt} = \min. \left\{ 0.544 t_{\text{sd}}, \frac{1.46 h^4}{\sin^3(t_{\text{sd}}/2)} \right\} \frac{1}{t_{\text{wav}}} \quad (12)$$

where

$$t_{\text{wav}} = \frac{M}{\mu} \frac{M}{\Sigma} \frac{h^4}{r^2 \omega_{\text{K}}}, \quad (13)$$

It is straightforward to see ω_{DI} reaches its maximum value

$$\omega_{\text{DI}}^{\text{max}} \approx \frac{h}{t_{\text{wav}}}, \quad (14)$$

at $t_{\text{sd}} \approx 2h$. The decoupling radius is determined by the equation $\omega_{\text{DI}}(r_{\text{dec}}) = \omega_{\text{DI}}^{\text{max}}(r_{\text{dec}})$ as

$$r_{\text{dec}} = 430 M_{\bullet} a^{1/8} \alpha_{0.1}^{1/8} \dot{M}_{\bullet, 0.1}^{1/2} \mu_{30}^{-1/8}, \quad (15)$$

for α disks, and

$$r_{\text{dec}} = 410 M_{\bullet} a^{10/59} \alpha_{0.1}^{8/59} \dot{M}_{\bullet, 0.1}^{24/59} M_{\bullet, 6}^{-2/59} \mu_{30}^{-10/59}, \quad (16)$$

for β disks, where we have defined $\mu_{30} = \mu/30M_{\odot}$, $M_{\bullet, 6} = M_{\bullet}/10^6 M_{\odot}$, $\dot{M}_{\bullet, 0.1} = \dot{M}_{\bullet}/0.1 \dot{M}_{\bullet, \text{Edd}}$ and we have used analytic models of α and β disks [12, 13]. The two numerical factors are nearly equal because the two disk models are similar at large radii where the gas pressure dominates the total pressure in the accretion disk. Due to the sharp r dependence of the two rates ω_{LT} and ω_{DI} , the decoupling radius r_{dec} turns out to be insensitive to M_{\bullet} , α , m , and only has a mild dependence on the SMBH accretion rate \dot{M}_{\bullet} . From Eq. (11), it is straightforward to see that the SMO is nearly aligned with the disk ($\vec{L}/L \approx \vec{n}_{\text{disk}}$) for $r > r_{\text{dec}}$ and starts to precess around the SMBH spin axis at $r < r_{\text{dec}}$. The transition between the two regimes is very sharp due to the sharp r dependence of the two rates ω_{LT} and ω_{DI} .

As an sBH crosses an accretion disk with relative velocity v_{rel} higher than the local gas sound speed v_s , the gas within the accretion radius $r_{\text{acc}} := 2Gm/v_{\text{rel}}^2$ will be shocked and the total orbital energy loss of the sBH per collision turns out to be [65]

$$\begin{aligned} \delta E_{\text{sBH}} &= 4\pi \ln \Lambda \frac{G^2 m^2}{v_{\text{rel}}^2} \frac{\Sigma}{\sin(t_{\text{sd}})}, \\ &\approx 2 \times 10^{46} \text{ ergs} \left(\frac{\ln \Lambda}{10} \right) \Sigma_5 \mu_{30}^2 r_{100} \left(\frac{\sin t_{\text{sd}}}{0.1} \right)^{-3}, \end{aligned} \quad (17)$$

where ι_{sd} is the angle of inclination between the EMRI orbital plane and the disk plane, and we have defined $\Sigma_5 = \Sigma/10^5 \text{ g cm}^{-3}$, $r_{100} = r/100M_\bullet$. In the α -disk and the β -disk models, the disk surface densities are formulated as

$$\Sigma(r) = 1.7 \times 10^5 \text{ g cm}^{-2} \alpha_{0.01}^{-1} \dot{M}_{\bullet,0.1}^{-1} r_{100}^{3/2}, \quad (18)$$

and

$$\Sigma(r) = 5.0 \times 10^5 \text{ g cm}^{-2} \alpha_{0.1}^{-4/5} \dot{M}_{\bullet,0.1}^{3/5} M_{\bullet,6}^{1/5} r_{100}^{-3/5}, \quad (19)$$

respectively. Therefore, wet EMRI with a warped disk is a natural mechanism to generate type II QPEs. If type II QPEs are confirmed in future observations, their existence provides indirect evidence for warped disks and the chaotic accretion mode in AGNs.

As the EMRI enters the LISA sensitivity band with orbital radius $r \sim 10M_\bullet$ and orbital frequency $f_{\text{obt}} \sim \text{mHz}$, the energy budgets per collision for two disk models are quite different. In the α -disk model, it scales as $\delta E_{\text{SBH}} \propto r^{5/2} \propto f_{\text{obt}}^{-5/3}$, that is say, the mHz QPEs will be $O(10^3)$ times weaker than their low-frequency counterparts. Although the identification of mHz type II QPEs is difficult in a sea of much stronger AGN variability, the joint GW measurement of the orbits may help identify the detection of mHz type II QPEs. If the accretion disk can be modeled as a β -disk, the energy budget per collision scales as $\delta E_{\text{SBH}} \propto r^{2/5} \propto f_{\text{obt}}^{-4/15}$, i.e. the mHz QPEs will be a few times weaker than their low-frequency counterparts. In this case, the identification of mHz QPEs is possible even without the input of GW observations. This multi-messenger source will be a convenient probe to accretion physics, e.g., distinguishing the two disk models and inferring the magnitude of the commonly used but not well constrained α parameter.

The other possible phenomenon to observe is the strong lensing of flares processed by the central SMBH, similar to self-lensing flares from SMBH binaries [73]. In this case, the strong lensing of the EMRI-produced flares is probably more likely to happen because the sBH is much closer to its host. As shown in [74], the strong lensing probability of a flare (either an EM flare or GWs) emitted at radius r is approximately

$$P_{\text{strong lensing}} \approx \frac{M_\bullet}{4r}. \quad (20)$$

Therefore the chance of strong lensing of a single flare is around $O(1\%)$ level, and the chance will be largely enhanced considering multi-flares are produced as the EMRI orbiting around the SMBH and crossing the accretion disk at different locations. Unlike the case of SMBH binaries with one of them hosting a mini-accretion disk where the background light source is stable and the variations in the light curve mainly come from when the mini disk gets lensed by the foreground BH, the light curve of mHz QPEs varies from flare to flare even without lensing. A more detailed study is required to confirm whether the lensing effect can be identified from the QPE light curve.

To summarize, wet EMRIs are promising sources of EM transients (dubbed as type II QPEs). If confirmed, they can

be used as a probe to AGN disk structure, and their existence provides indirect evidence for warped AGN disks and chaotic AGN accretion. In addition, wet EMRIs in the mHz band will be emitting multi-messenger signals that are possibly detectable by both spaceborne GW detectors and X-ray telescopes, where there is a chance that the X-ray flares get lensed by the SMBH.

C. Calibrating other Methods of Probing Black Hole Mass and Spin

z	M_\bullet M_\odot	λ_{Edd}	$\kappa_{2-10 \text{ keV}}$ erg s^{-1}	$L_{2-10 \text{ keV}}$	$F_{2-10 \text{ keV}}$ $\text{erg s}^{-1} \text{ cm}^{-2}$
0.1	1.0×10^6	0.2	20	1.3×10^{42}	5.1×10^{-14}
0.1	2.0×10^6	0.1	30	8.7×10^{41}	3.4×10^{-14}
0.1	5.0×10^6	0.2	70	1.9×10^{42}	7.3×10^{-14}
0.1	5.0×10^6	0.5	125	2.6×10^{42}	1.0×10^{-13}
0.2	1.0×10^6	0.2	20	1.3×10^{42}	1.1×10^{-14}
0.3	1.0×10^6	0.2	20	1.3×10^{42}	4.5×10^{-15}

TABLE II. Exemplary estimations of the 2–10 keV X-ray luminosity and flux for SMBH counterparts at redshift $z = 0.1$.

The mass and spin measurements of SMBHs in AGNs have been a long-standing challenge. Standard techniques involving spatially resolved kinematics of stars or the $M_\bullet - \sigma_\star$ relation [77] generally are not applicable because the strong AGN continuum has seriously diluted any features of stars [78, 79]. GWs provide precise (better than 0.1% [2]) measurements of the mass and even spin of SMBHs, which can be used to calibrate traditional EM wave methods. For this purpose, wet EMRIs that take place in type I AGNs are favored, as traditional measurements based on AGN features all have large uncertainties and thus require improved calibration.

To estimate the fraction of wet EMRIs that could be used for such calibration, the active type I fraction of galaxies was estimated in a two-step process. First, following [80], we adopt the active ($\lambda_{\text{Edd}} > 10^{-3}$) fraction of $\sim 15 - 40\%$ for galaxies with $5.5 < \log_{10}(M_\bullet) < 6.5$, where λ_{Edd} is the Eddington ratio. This is broadly consistent with the active fraction of $\sim 24 - 34\%$ for the same BH mass range estimated by [81], although a lower Eddington ratio is adopted. The active fraction of [80] is comparable to that of $\sim 10 - 16\%$ for a larger BH mass range $6.5 < \log_{10}(M_\bullet) < 10.5$ [82], where the same Eddington ratio is adopted. Furthermore, [83] yielded an active fraction of $\sim 10 - 22\%$ for the host galaxy stellar mass range $9.0 < \log_{10}(M_{\star, \text{host}}) < 10.0$. Assuming a $M_\bullet - M_{\star, \text{host}}$ relation (e.g., Eq. 39 of [80]), this translates to a BH mass range of $5.0 < \log_{10}(M_\bullet) < 6.0$. Second, the active fraction of [80] should be multiplied by the type I fraction of active galaxies. The type I fraction of active galaxies ranges from $\sim 7\%$ [84] to $\sim 20\%$ [85, 86]. Therefore, the active type I fraction of galaxies is $\sim 1 - 8\%$ [80]. This is comparable to that of $\sim 4\%$ for a larger BH mass range

TABLE III. Catalog of selected SMBHs with masses below $10^7 M_\odot$, whose mass and spin have been determined through EM observations. All masses are reported with 1σ errors (if provided), while spins are reported with 90% error ranges. The SNRs are calculated at a fixed source redshift ($z = 0.3$ [75]) using four years of data from various detectors. According to the work by Babak et al. [2], the measurement uncertainties for the mass and spin of the SMBH could range from approximately $10^{-6} \sim 10^{-4}$ and $10^{-6} \sim 10^{-3}$, respectively.

Object	Mass [$\times 10^6 M_\odot$]	Spin	z	SNR ($z = 0.3$)			Alternate Names
				LISA [52, 53]	TianQin [7]	TaiJi [76]	
UGC 01032	~ 1.1	$0.66^{+0.30}_{-0.54}$	0.01678	87	56	280	Mrk 359
UGC 12163	~ 1.1	> 0.9	0.02468	92	61	290	Ark 564
Swift J2127.4+5654	~ 1.5	0.6 ± 0.2	0.01400	66	38	210	
NGC 4253	$1.8^{+1.6}_{-1.4}$	> 0.92	0.01293	64	37	200	UGC 07344, Mrk 766
NGC 4051	1.91 ± 0.78	> 0.99	0.00234	33	19	110	UGC 07030
NGC 1365	~ 2	> 0.97	0.00545	29	16	92	
1H0707-495	~ 2.3	> 0.94	0.04056	19	11	63	
MCG-6-30-15	$2.9^{+1.8}_{-1.6}$	$0.91^{+0.06}_{-0.07}$	0.00749	10	6.8	36	
NGC 5506	~ 5	0.93 ± 0.04	0.00608	3.0	2.3	11	Mrk 1376
IRAS13224-3809	~ 6.3	> 0.975	0.06579	1.7	1.5	6.6	
Ton S180	~ 8.1	> 0.98	0.06198	0.9	0.9	3.7	

$6.5 < \log_{10}(M_\bullet) < 10.5$ [82]. Hence, merely a few percent of wet EMRIs could be used to calibrate traditional X-ray measurements of the SMBH spin and optical measurements of the SMBH mass.

For optical counterparts of such wet EMRI, the most commonly used method to estimate M_\bullet is the so-called virial mass estimator, which is based on costly and time-consuming reverberation mapping or convenient yet less accurate single-epoch spectra [87, 88]. It assumes that the regions emitting broad emissions, known as broad-line region (BLR) clouds, are entirely governed by the gravitational force of the BH, so that M_\bullet can be measured as long as the velocity (v) and distance (r) of the BLR clouds from the BH are known, i.e. $M_\bullet = f \frac{rv^2}{G}$. There is a uniformly assigned coefficient f in the calculation, which is calibrated by the $M_\bullet - \sigma_\star$ relation, assuming that active and inactive galaxies follow the same relation. Note that the intrinsic scatter of the tightest $M_\bullet - \sigma_\star$ relation for local massive galaxies is at least $0.3 - 0.5$ dex [77, 89, 90], the uncertainty associated with the f used for AGNs could be considerably larger. Moreover, for a given AGN, it suffers from additional uncertainties from the kinematics, geometry, inclination of the clouds, and even the nature of the bulges [91], making the real f hugely different from object to object. Recently, some exciting progress has been made with the advanced NIR interferometry GRAVITY, mounted on the Very Large Telescope Interferometer (VLTI), which has shown promise in probing the BLR structure and thus improving the precision of the M_\bullet measurement [92, 93]. Unfortunately, it can only be applied to very few near-infrared luminous AGNs.

For X-ray counterparts of such wet EMRIs in type I AGNs, the most commonly used method to estimate BH spin is X-ray reflection spectroscopy [94, 95]. The reflection spectroscopy takes advantage of the skewed line profile of the 6.4 keV

Fe line, which is featured with a sharp blueshifted peak due to the relativistic beaming effect and an extended redshifted wing due to the gravitational redshift of matter close to the innermost stable circular orbit (ISCO). More technical details, as well as descriptions of other techniques, can be found in the recent review on the observational constraints on BH spin [96].

For those active type I galaxies with wet EMRI signals, their 2 – 10 keV luminosity is estimated as

$$L_{2-10 \text{ keV}} = 1.3 \times 10^{44} \left(\frac{M_\bullet}{10^6 M_\odot} \right) \left(\frac{\lambda_{\text{Edd}}}{\kappa_{2-10 \text{ keV}}} \right) \quad (21)$$

where M_\bullet is the BH mass, λ_{Edd} the Eddington ratio, $\kappa_{2-10 \text{ keV}}$ the 2 – 10 keV bolometric correction. The ratio of $\lambda_{\text{Edd}}/\kappa_{2-10 \text{ keV}}$ is in the range of $0.001 - 0.1$ [97]. Generally speaking, $\kappa_{2-10 \text{ keV}} \sim 20 - 70$ for $0.1 < \lambda_{\text{Edd}} < 0.2$ and $\kappa_{2-10 \text{ keV}} \sim 70 - 150$ for $\lambda_{\text{Edd}} > 0.2$ [98]. The 2 – 10 keV flux is obtained following the inverse square law of the luminosity distance, where we assume the standard flat Λ CDM cosmology with parameters $H_0 = 70 \text{ km s}^{-1} \text{ Mpc}^{-1}$ and $\Omega_m = 1 - \Omega_\Lambda = 0.3$. Table II lists exemplary estimations, mainly for $z = 0.1$. The estimated 2 – 10 keV X-ray flux is low in general ($\lesssim 10^{-13} \text{ erg s}^{-1} \text{ cm}^{-2}$) but detectable. For comparisons, the XMM-COSMOS survey can reach the 2 – 10 keV flux limit of $\sim 9.3 \times 10^{-15} \text{ erg s}^{-1} \text{ cm}^{-2}$, with an average vignetting-corrected exposure of 40 ks [99]. To estimate the BH spin, merely detection is not enough. Ideally, it is preferable to match the spectral quality of the nearby AGN with the BH spin measurement [96]. For comparisons, the 2 – 10 keV flux of Mrk 359 ($z = 0.01678$, [100]) listed in Table III is $\gtrsim 5 \times 10^{-12} \text{ erg s}^{-1} \text{ cm}^{-2}$. For the X-ray counterparts of wet EMRIs, it is essential to take deep-exposure observations using future X-ray missions (e.g., eXTP [101] and Athena [102]) with significantly larger effective areas than those of current

missions.

Table III presents a catalog of selected SMBHs with masses below $10^7 M_\odot$, whose masses and spins have been determined using EM observations [96, 103, 104]. The table also includes SNRs for GW detections from LISA, TianQin, and Taiji, assuming a source with the same intrinsic parameters placed at the redshift of $z = 0.3$ and with four years of observation. Although EM observations of SMBH spin typically carry significant uncertainties due to the limitations of current methods, GW observations from wet EMRIs provide far greater precision, with uncertainties as low as $10^{-6} \sim 10^{-4}$ for mass and $10^{-6} \sim 10^{-3}$ for spin [2]. This comparison highlights the potential of wet EMRIs to calibrate traditional EM techniques, which rely on indirect methods such as X-ray reflection or virial mass estimators, often affected by large scatter and systematic biases. By integrating EM and GW data, Table III illustrates the critical role of wet EMRIs in improving the accuracy and reliability of SMBH mass and spin measurements, especially in type I AGNs.

D. Testing Accretion Disk and Jet Models

Astrophysical jets, such as those observed in AGN and X-ray binaries, are often believed to be launched through two primary theoretical mechanisms or their variants: the Blandford-Znajek (BZ) mechanism and the Blandford-Payne (BP) mechanism, which differ in their energy sources and jet-launching regions.

With the BZ mechanism [105] a jet extracts energy and angular momentum from a spinning SMBH through magnetic fields that thread its event horizon. This process converts the rotational energy of the BH into jet power via the Penrose process [106] to jet energy, so that the direction of the jet should be highly correlated with the spin axis of the BH \hat{a} .

In contrast, through the BP mechanism [107] a jet extracts energy from the rotational motion of the accretion disk via magnetic fields that thread the disk. These fields centrifugally accelerate material along magnetic field lines and collimate it into a jet [108]. The resulting jet aligns with the direction of the disk magnetic field, which should be highly correlated with the angular momentum \hat{L}_{disk} . Notice that \hat{L}_{disk} may differ from \hat{a} due to disk warping or misalignment, as discussed in Sec. II B.

Understanding the directional relationships among the accretion disk \hat{L}_{disk} , the SMBH spin axis \hat{a} , and the jet direction (as illustrated in Fig. 2) is crucial for interpreting the jet-launching process. These relationships not only help disentangle the dominant jet-launching mechanism but also provide insights into the interplay between BH spin, accretion disk dynamics, and magnetic fields.

The spin axis of the SMBH (\hat{a}) is the most straightforward to measure of the three vectors, thanks to the exceptional precision of GW observations. GW observations offer precise measurements of the SMBH's spin, including both its magnitude and direction, with an accuracy ranging from $10^{-6} \sim 10^{-3}$ [2], which is more than three orders of magnitude better than the precision achieved through EM obser-

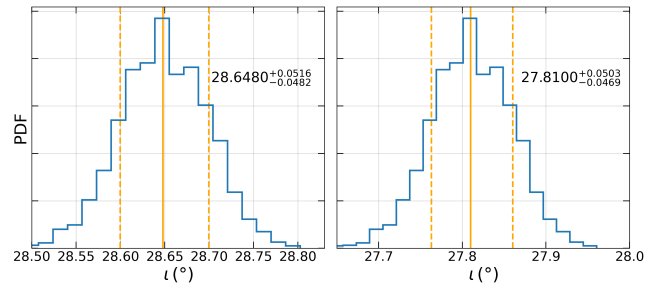


FIG. 1. Posterior distribution of the inclination angle ι , with the dimensionless semi-latus rectum $p_0 \sim 8M_\bullet$ (left panel) and traced back to $p \sim 150M_\bullet$ (right panel). The orange vertical lines indicate the mean value along with the $1 - \sigma$ uncertainty.

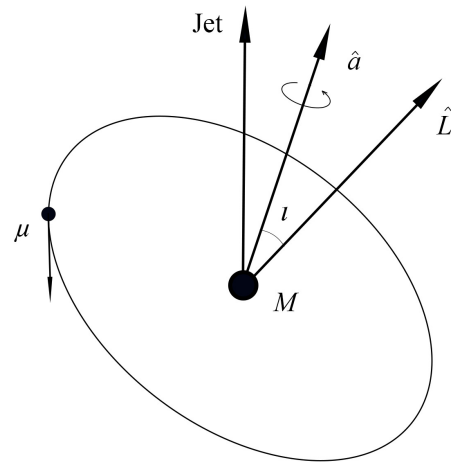


FIG. 2. The relationship among the orbital angular momentum of the sBH \hat{L} , the SMBH spin direction \hat{a} , and the jet angle. The disk orientation \hat{L}_{disk} is inferred by tracing \hat{L} backward from the LISA band ($p_0 \sim 8M_\bullet$) to $p \sim 150M_\bullet$, where the sBH resides within the disk.

ations (as summarized in Table III). Moreover, GW signals provide highly accurate measurements of the inclination angle ι , which represents the angle between the SMBH spin axis (\hat{a}) and the orbital angular momentum vector (\hat{L}), at $p \sim 8M_\bullet$, corresponding to the LISA band.

In the warped disk scenario, determining the orientation of the accretion disk (\hat{L}_{disk}) is more challenging, as the evolution of sBH depends on a complex interplay of forces acting at different radii. In the outer regions of the disk, the motion of the sBH is primarily governed by disk forces, while closer to the SMBH, GW radiation dominates its evolution. At larger radii, the sBH moves within the plane of the disk, but as it approaches smaller radii, it gradually departs from the disk due to Lense-Thirring precession induced by the SMBH [109].

To reconstruct the orientation of the accretion disk at larger radii, GW measurements of the orbital configuration of sBH in the LISA band (with $p \sim 8M_\bullet$) can be used as a starting point to evolve the system backward to $p \sim 150M_\bullet$, where the GW lifetime becomes 0.5 Myrs and the disk forces begin

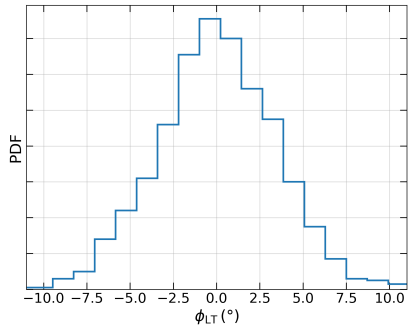


FIG. 3. The uncertainty in the Lense-Thirring precession angle at $p \sim 150M_\bullet$, traced back from a semi-latus rectum of $p_0 \sim 8M_\bullet$.

to dominate. For simplicity, in this backward evolution, we take a crude approximation that GW damping is the only mechanism that governs the dynamics of the system. At $p \sim 150M_\bullet$, the orientation of the disk, influenced by Lense-Thirring precession, can be decomposed into two components: the angle of inclination relative to the SMBH spin axis and the angle of precession, which describes its azimuthal orientation. This approach enables a reconstruction of the orientation of the disk and provides critical insights into its role in the jet-launching process.

To determine the inclination angle of the accretion disk relative to the SMBH's spin, we first estimate the inclination angle ι , defined as [110]

$$\cos \iota = \frac{L_z}{\sqrt{Q + L_z^2}}, \quad (22)$$

where L_z represents the z -component of the orbital angular momentum of the sBH, and Q is the Carter constant. The inclination angle ι represents the orientation of the orbital angular momentum relative to the spin of SMBH. However, as ι increases over time due to the radiation reaction [111–113], it no longer reliably indicates the orientation of the accretion disk. To estimate the disk's orientation, the orbital trajectory must be evolved backward to regions far from the SMBH, where ι can, in principle, reflect the orientation of the accretion disk.

The measurement uncertainty of ι as the EMRI system enters the LISA band ($p_0 \sim 8M_\bullet$) is estimated by performing Fisher analysis with the Augmented Analytic Kludge (AAK) waveform model [46, 47]. Fisher analysis is a well-established statistical method for quantifying the precision with which GW observatories, such as LISA, can extract source parameters from observed signals. The Fisher information matrix, Γ_{ij} , is defined as:

$$\Gamma_{ij} = \left\langle \frac{\partial h}{\partial \lambda_i}, \frac{\partial h}{\partial \lambda_j} \right\rangle, \quad (23)$$

where h is the signal, λ_i are the source parameters, and the inner product is defined by Eqn. 7. The covariance matrix, $\Sigma_{ij} = (\Gamma^{-1})_{ij}$, is obtained by inverting the Fisher matrix, with

the diagonal elements, $\sigma_{\lambda_i}^2 = \Sigma_{ii}$, quantify the variances of the parameters.

The posterior samples obtained from this analysis are propagated backward by evolving the orbital trajectory to $p \sim 150M_\bullet$, where the orbital angular momentum of the sBH provides an estimate of the accretion disk's orientation and, consequently, the angle relative to the SMBH's spin. As an example, we use a simulated EMRI system with the following key parameters:

- SMBH mass: $M_\bullet = 10^6 M_\odot$
- SMBH spin: $a = 0.98$
- stellar BH mass: $\mu = 10 M_\odot$
- initial eccentricity: $e = 0.01$
- observation time: $T = 2$ years
- inclination angle: $\iota \approx 30^\circ$
- SNR: fixed at 50 by adjusting the luminosity distance

As shown in Fig. 1, the $1 - \sigma$ uncertainty for the inclination angle is approximately $\sim 0.05^\circ$. This angle corresponds to the inclination of the warped accretion disk at the decoupling radius ($p \sim 150M_\bullet$), where the influence of disk torques begins to dominate over GW radiation. This result demonstrates that GWs provide a highly precise measurement of the disk's inclination at the critical decoupling radius, as discussed in Sec. II B.

On the other hand, to estimate the uncertainty in the precession angle at the decoupling radius, we perform similar analysis to propagate samples of orbital configurations measured at $p_0 \sim 8M_\bullet$ (within the LISA band) backward to a semi-latus rectum of $p \sim 150M_\bullet$, where the orbital direction is measured. It is much larger than R_{warp} (see Eq. 8) so $p \sim 150M_\bullet$ already corresponds to the outer-disk region. The uncertainties in the precession angle grow approximately linearly with increasing p , reaching a value of around 10° at $p \sim 150M_\bullet$ as shown in Fig. 3. This level of uncertainty makes it challenging to resolve the azimuthal orientation of the warped disk.

In addition to GW-derived measurements of the SMBH spin and the inclination angle, EM observations can estimate the jet direction if the host AGN of the EMRI is resolvable. For AGNs with jet viewing angles smaller than $\sim 10^\circ$, radio observations, such as those conducted by the MOJAVE program, can determine the jet angle with an accuracy of approximately 1° by analyzing jet kinematics [114–121]. Furthermore, for gamma-ray bright AGNs, observations from *Fermi*-LAT typically measure larger jet viewing angles and greater accuracy on average compared to non-LAT-detected AGNs [115, 118].

The interplay between the jet direction, the SMBH spin axis, and the orientation of the accretion disk will likely provide critical information to understand the mechanisms of accretion and jet launch in AGN. As shown in Fig. 2, GW signals enable precise measurements of the SMBH spin axis and the inclination angle ι , and hence the orientation of the accretion disk relative to the SMBH spin. EM observations, on the other hand, can determine the jet direction. Although this allows for an estimation of the relative angle between the jet and the SMBH spin axis, the angle between the jet and the

accretion disk orientation remains inaccessible because of the large uncertainty in the precession angle. This indirect relationship between the accretion disk orientation and the jet direction limits our ability to fully understand the correlations between these vectors. In addition, to statistically establish the correlations, it will likely require studying a population of wet EMRIs (those with significant disk interactions) with well-resolved EM counterparts.

E. Cosmology with Wet EMRIs

Wet EMRIs provide a promising avenue for probing cosmological models by serving as both “bright” and “dark” sirens. These systems combine GW measurements of the luminosity distance with EM observations to determine the redshift of their possible host galaxies. When the host galaxy can be unambiguously identified, wet EMRIs act as bright sirens, enabling an independent measurement of the Hubble parameter. However, to qualify as a bright siren, a wet EMRI requires high localization precision and a unique association with its host AGN.

To assess the feasibility of identifying bright sirens, we analyze catalogs of wet EMRIs generated from various astrophysical models (see Table I), such as an α -disk model with $T_{\text{disk}} = 10^6$ years. For each EMRI system, Fisher analysis is employed to estimate the number of potential host galaxies within its localization volume. The solid angle uncertainty, $\Delta\Omega_s$, derived from the Fisher matrix components associated with the angular parameters (θ_s, ϕ_s) , is expressed as (see also [75, 122]):

$$\Delta\Omega_s = 2\pi \sin \theta_s \sqrt{\Sigma_{\theta_s, \theta_s} \Sigma_{\phi_s, \phi_s} - (\Sigma_{\theta_s, \phi_s})^2}, \quad (24)$$

where $\Sigma_{ij} = (\Gamma^{-1})_{ij}$ is the covariance matrix obtained as the inverse of the Fisher information matrix Γ_{ij} . This covariance matrix quantifies the uncertainties and correlations in the angular parameters. To estimate the volume of three-dimensional localization (V_{sky}) in spherical coordinate, the uncertainty of the solid angle is combined with the uncertainty of the luminosity distance d_L . The localization volume is given by

$$V_{\text{sky}} = \frac{1}{2} r^3(z) \sigma(\ln d_L) \Delta\Omega_s, \quad (25)$$

where $r(z)$ is the comoving distance to the source as a function of redshift, and $\sigma(\ln d_L)$ is the relative uncertainty in the distance measurement. For LISA-detected EMRIs, Fisher analysis indicates that V_{sky} can be restricted to $\mathcal{O}(10^2) \text{ Mpc}^3$ at moderate redshifts ($z < 0.3$), depending on the SNR and the inclusion of higher order waveform harmonics, demonstrating the high localization precision of LISA.

After applying a conservative AGN fraction ($f_{\text{AGN}} = 1\%$), we operationally classify an EMRI as a bright siren if the expected number of AGNs within this volume is less than 1.1. Across various models in Table I, we find that approximately 20% \sim 25% of detectable wet EMRIs have resolvable host galaxies, translating to a detection rate of 3 \sim 30 bright sirens

per year. However, not all wet EMRIs meet this criterion. Those systems with multiple potential AGN hosts within the localization volume are classified as dark sirens, indicating ambiguity in host galaxy association.

Dark sirens, despite the absence of unambiguous host galaxy identification, still play a significant role in measuring the Hubble parameter. In such cases, statistical methods can be employed, utilizing galaxy catalogs to infer redshift distributions within the localization volume. Although this approach offers reduced precision compared to bright sirens, it enables dark sirens to complement bright sirens in constraining cosmological parameters, as dark sirens primarily use EMRIs with higher redshift than bright sirens. In addition, to account for observational challenges, such as interstellar extinction or incomplete AGN catalogs, we conservatively reclassify 10% of the initially identified bright sirens as dark sirens.

In summary, wet EMRIs offer a unique opportunity to probe the Hubble parameter through bright and dark sirens. Bright sirens provide precise, independent measurements when host galaxies are resolvable, while dark sirens contribute through statistical inference methods. The following sections will explore the respective roles of bright and dark sirens in constraining the Hubble parameter.

1. Wet EMRIs as bright sirens

The groundbreaking detection of GW170817, with its well-identified host galaxy (NGC 4993) and associated kilonova AT 2017gfo, marked the first GW-based measurement of the Hubble constant, yielding $H_0 = 70.0_{-8}^{+12} \text{ km s}^{-1} \text{ Mpc}^{-1}$ [123]. This pioneering result demonstrated the potential of joint GW and EM observations to independently constrain cosmological parameters. Building on this framework, wet EMRIs represent another promising class of bright sirens, particularly in the context of future cosmological studies.

Wet EMRIs, which involve compact objects spiraling into SMBHs within AGN disks, are ideal candidates for joint GW-EM observations. Similar to past events such as GW170817, wet EMRIs can act as bright sirens if their host AGNs are uniquely identified, allowing for precise redshift measurements. In addition, wet EMRIs have several advantages over other sources, such as binary neutron star or neutron star–black hole mergers. These advantages include higher expected detection rates, the ability to probe greater cosmological distances, and robust EM counterparts. Their relatively high localization precision and strong association with AGNs allow for a confident identification of host galaxies and their corresponding redshifts, making them powerful tools for constraining H_0 and other cosmological parameters at cosmological scales.

To measure H_0 using wet EMRI bright sirens, the luminosity distance d_L obtained from GW signals is combined with the redshift z of the host AGN. Assuming a flat Λ CDM cosmology, the relationship between luminosity distance and red-

shift ($d_L - z$ relation) is expressed as

$$d_L(z) = c(1+z) \int_0^z \frac{dz'}{H(z')}, \quad (26)$$

where the Hubble parameter, $H(z)$, is given by

$$H(z) = H_0 \sqrt{\Omega_{m,0}(1+z)^3 + \Omega_{\Lambda,0}}, \quad (27)$$

and $\Omega_{m,0}$ and $\Omega_{\Lambda,0}$ are the present-day matter and dark energy densities, respectively, satisfying $\Omega_{m,0} + \Omega_{\Lambda,0} = 1$. The present value of the Hubble parameter, H_0 , can be expressed in terms of the dimensionless parameter h , such that $H_0 = h \times 100 \text{ km s}^{-1} \text{ Mpc}^{-1}$.

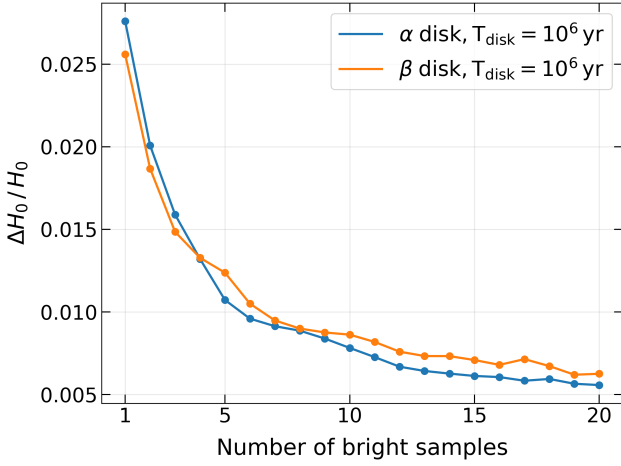


FIG. 4. The $1\text{-}\sigma$ relative uncertainty of the Hubble parameter H_0 as a function of the number of bright EMRIs is shown for two representative wet EMRI models. As expected, the uncertainty on H_0 decreases with increasing numbers of bright EMRIs, reaching 1% with seven bright sirens. Other simulated wet EMRI models exhibit similar behavior. The colored dots represent the calculated data points

For each EMRI model listed in Table I, the Hubble parameter H_0 can be constrained by statistically combining the luminosity distance derived from GW, d_L , and its associated uncertainty, $\sigma(d_L)$, with the redshift of the host AGN. To achieve this, we randomly sample N bright sirens from the catalog corresponding to the chosen EMRI model and perform Markov-Chain Monte Carlo (MCMC) simulations to derive the posterior distributions of dimensionless Hubble parameter h and other cosmological parameters, such as matter density $\Omega_{m,0}$.

To reduce the effects of randomness in the sampling process, this procedure is repeated 90 times for each value of N . By averaging the results across these repetitions, we estimate the mean value of H_0 and its corresponding uncertainty, ΔH_0 , ensuring statistical robustness. This approach ensures that the constraints derived from H_0 are reliable and representative of the underlying EMRI population for the selected astrophysical model.

Fig. 4 shows the $1\text{-}\sigma$ relative uncertainty in H_0 as a function of the number of bright EMRIs, based on two representative

wet EMRI models. As expected, the uncertainty on H_0 decreases as the number of bright EMRIs increases. The results suggest that with approximately seven bright EMRI detections, H_0 can be restricted to within 1% uncertainty. This level of precision is comparable to that achieved using EM standard candles, such as Type Ia supernovae [124], and has the potential to help resolve the ‘‘Hubble tension’’ between early- and late-universe H_0 measurements. Furthermore, the higher redshifts accessible to wet EMRIs provide an opportunity to probe additional cosmological parameters, such as the matter density $\Omega_{m,0}$ and the dark energy equation of state parameter.

The inclusion of wet EMRI bright sirens in cosmological studies enhances the scope of GW-based standard siren measurements, complementing those from BNS and BBH mergers. Future multimessenger detections will enable combined constraints from bright sirens across various GW source classes, significantly refining measurements of H_0 and other cosmological parameters. This, in turn, will deepen our understanding of the expansion history of the universe and the underlying physics of dark energy.

2. Wet EMRIs as dark sirens

The dark siren analysis technique is a powerful statistical method for inferring cosmological parameters from GW events that lack identifiable EM counterparts. Instead of requiring a uniquely resolved host galaxy, this approach utilizes the spatial localization of the GW source and statistically matches it with the galaxy or AGN catalogs [125, 126]. By assigning probabilities to potential host galaxies within the GW localization volume, the technique extracts redshift information and combines it with the GW-derived luminosity distance to constrain parameters such as the Hubble parameter H_0 . This method is particularly well-suited for EMRIs or BBH mergers that lack direct observable EM counterparts.

The technique operates within the framework of Bayesian inference. For a set of GW events $D = \{D_1, \dots, D_N\}$, the posterior distribution of the cosmological parameters $\Theta = \{H_0, \Omega_{m,0}, \dots\}$ is given by

$$p(\Theta | D, \mathcal{H}, I) = \frac{p(D | \Theta, \mathcal{H}, I) p(\Theta | \mathcal{H}, I)}{p(D | \mathcal{H}, I)}, \quad (28)$$

where \mathcal{H} is the assumed cosmological model, I represents prior information, and $p(\Theta | \mathcal{H}, I)$ is the prior on the parameters. The evidence $p(D | \mathcal{H}, I)$ serves as a normalization constant, while the likelihood $p(D | \Theta, \mathcal{H}, I)$ encodes the probability of the data given the parameters. For a single GW event, the likelihood is expressed as

$$p(D_i | \Theta, \mathcal{H}, I) = \int \int dz_{\text{gw}} dd_L p(d_L | z_{\text{gw}}, \Theta, \mathcal{H}, I) p(z_{\text{gw}} | \Theta, \mathcal{H}, I) p(D_i | d_L, z_{\text{gw}}, \Theta, \mathcal{H}, I), \quad (29)$$

where d_L is the luminosity distance, z_{gw} is the redshift of the GW source, and $p(d_L | z_{\text{gw}}, \Theta, \mathcal{H}, I) = \delta(d_L - d(z_{\text{gw}}, \Theta))$ relates

the luminosity distance to the redshift through the assumed cosmological model. The term $p(z_{\text{gw}} | \Theta, \mathcal{H}, I)$ represents the prior probability of the source redshift, which is informed by the galaxy catalog. The final term, $p(D_i | d_L, z_{\text{gw}}, \Theta, \mathcal{H}, I)$, is the likelihood of GW data, which is typically modeled as a Gaussian centered on the observed d_L with uncertainties from GW parameter estimation and weak lensing [127].

Although the general dark-siren method applies to all GW events, wet EMRIs offer a distinct advantage due to their strong association with AGNs. For BBH mergers, all galaxies within the error volume of a single GW event must be considered as potential hosts. In contrast, for wet EMRIs, the search is limited to galaxies that host AGNs (we conservatively take an AGN fraction $f_{\text{AGN}} = 1\%$), significantly reducing the number of candidates. This reduction improves the statistical association between the GW source and its host galaxy, leading to tighter constraints on cosmological parameters.

To statistically associate host galaxies with the GW source, the redshift prior $p(z_{\text{gw}} | \Theta, \mathcal{H}, I)$ is constructed by summing over all potential hosts - specifically, the host AGN galaxies in this study - within the GW localization volume:

$$p(z_{\text{gw}} | \Theta, \mathcal{H}, I) \propto \sum_{j=1}^{N_g} w_j \exp\left(-\frac{(z_j - z_{\text{gw}})^2}{2\sigma_{z,j}^2}\right), \quad (30)$$

where N_g is the number of candidate host galaxies, z_j is the catalog redshift of the j -th galaxy, $\sigma_{z,j}$ includes uncertainties from peculiar velocities and w_j is the weight assigned to each galaxy based on its spatial position to the GW sky localization.

As summarized in Table I, the wet EMRI models used predict the detection of 10–150 events per year, and most of the host AGNs are still poorly identified. For dark siren analysis, we adopt the first model (a α -disk model with $T_{\text{disk}} = 10^6$ years) as an example. This model predicts approximately 100 wet EMRIs per year with unresolvable host AGNs. In this simulation, we randomly select 30 dark EMRIs from the first model’s catalog to constrain the Hubble parameter H_0 . The sample size allows us to study a representative sample of the dark EMRI population while maintaining computational efficiency.

Each dark EMRI event is matched with an AGN catalog, using the reduced number of AGNs within the GW localization volume to build a redshift prior to dark siren analysis. The GW localization volume of each dark EMRI typically contains $\mathcal{O}(10^2) \sim \mathcal{O}(10^3)$ potential host galaxies. However, considering that only about 1% of galaxies host AGNs, the pool of candidate AGNs is reduced to $\mathcal{O}(10) \sim \mathcal{O}(10^2)$. This reduction significantly improves the statistical association between the source of GW and its host AGN compared to dry EMRIs, resulting in tighter constraints on H_0 and other cosmological parameters. By statistically matching the 30 selected dark EMRIs with AGN catalogs, the Hubble parameter can be constrained to 3% precision, as shown in Fig. 5. This level of precision, while slightly less than that achieved with bright sirens, underscores the power of dark sirens for independent cosmological measurements.

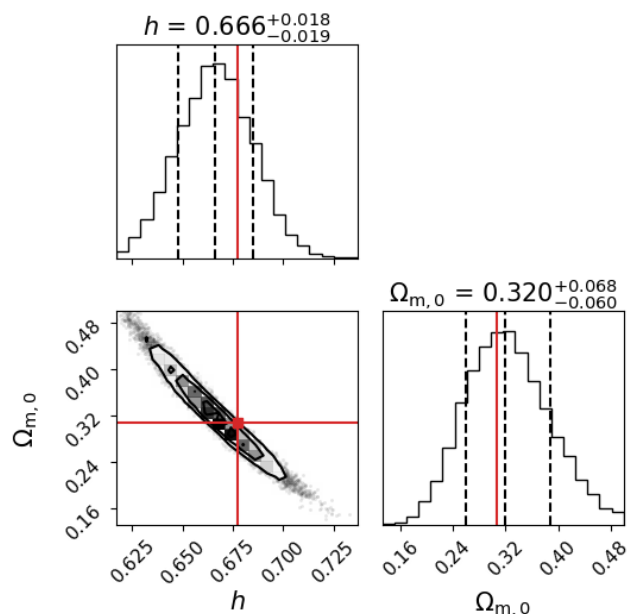


FIG. 5. Posterior distributions of the dimensionless Hubble parameter h and matter density $\Omega_{m,0}$ inferred from 30 wet EMRI dark sirens randomly selected from the first α -disk model. The solid red lines represent the true values, while the dashed lines indicate the mean and 1- σ standard deviation of the distributions.

This method offers a promising pathway for advancing GW cosmology, particularly in scenarios where EM counterparts are absent. Furthermore, the combination of bright and dark sirens provides complementary constraints across different redshift ranges: bright sirens probe lower redshifts with uniquely identifiable hosts, while dark sirens extend measurements to higher redshifts using statistical associations. Together, these approaches not only enhance our ability to constrain H_0 and other cosmological parameters but also offer valuable insights into the “Hubble tension”—a significant discrepancy between early-universe H_0 measurements from the Cosmic Microwave Background (CMB)[128, 129] and late-universe measurements from standard candles like Cepheid-calibrated Type Ia supernovae[124, 130] or GW-EM observations [123, 131, 132]. This tension, which challenges the standard Λ CDM model, has spurred exploration of potential solutions, including modified gravity [133–140], alternative forms of dark energy [141–145], or unaddressed measurement systematics [146–150]. By combining the complementary strengths of bright and dark sirens, GW cosmology provides a robust and independent approach to addressing this critical cosmological puzzle, while also offering a more comprehensive understanding of the universe’s expansion history.

III. DISCUSSION AND CONCLUSION

The various science opportunities discussed in Sec. II are still subject to several caveats and uncertainties, two of which are highlighted below.

First, there are still theoretical uncertainties regarding the profile of the disk and the migration of stars and stellar-mass objects within the disk. Previously, most work assumed the thin-disk profile, although at larger radii additional heating from stars is included to balance out the gravitational instabilities [151]. However, it is still unclear how many embedded objects are present within the disk and how they modify the structure of the disk. Between the GW dominated region and the Broad-Line region, some work has suggested that the disk becomes clumpy and rather turbulent, which further affect both the migration of stellar-mass objects within the disk and the rate of capturing from the nuclear star cluster. Although eventually the quasi-equilibrium wet EMRI formation is mainly determined by the supply rate of sBHs to the nuclear star cluster [24] rather than by detailed migration dynamics, it is necessary to understand these underlying physical processes before one can make further quantitative predictions.

Second, in Sec. II we have made the implicit assumption that wet EMRIs are associated with *visible* AGNs. We have tried to include an estimation of the “dark” sources because of dust absorption, especially in the Hubble parameter measurement. There is, however, another scenario that the EMRI is brought to the vicinity of the massive BH because of disk migration, but the disk becomes quiescent during the time that this EMRI is observed by space-borne GW detectors. This scenario mainly affects wet EMRIs formed at the end of disk life cycles. If the lifetime of the disk is on average T_{disk} and the

wet EMRI formation rate for that disk-assisted system is approximately once per T_{EMRI} (see the discussion in [21]), then this effect may affect a fraction of $T_{\text{EMRI}}/T_{\text{disk}}$ wet EMRIs. A more detailed study of this effect may include the time-dependent formation rate of wet EMRIs as the system starts to deplete sBHs within the nuclear star cluster.

Despite these uncertainties, the multi-messenger aspects of wet EMRIs are still less explored, partly because their abundance has only started to be quantitatively studied in recent years [21, 23, 24]. The applications in EM transients, in calibrating disk mass and spin measurements, in testing disk and jet models, and in cosmology discussed in this work are likely still a small subset of what one can learn from multi-messenger observations of wet EMRIs. We believe there is significant scientific potential in studying joint science cases for wet EMRIs with GW and/or X-ray, optical and radio observations, as well as multiband events coming from stellar-mass binary mergers within AGN disks.

Acknowledgements— We thank Jian-Ming Wang and Lianggui Zhu for interesting discussions. Zhenwei Lyu is supported by “the Fundamental Research Funds for the Central Universities” and Leicester International Institute, Dalian University of Technology. This research has made use of the NASA/IPAC Extragalactic Database, which is funded by the National Aeronautics and Space Administration and operated by the California Institute of Technology.

-
- [1] P. Amaro-Seoane, H. Audley, S. Babak, J. Baker, E. Barausse, P. Bender, E. Berti, P. Binetruy, M. Born, D. Bortoluzzi, J. Camp, C. Caprini, V. Cardoso, M. Colpi, J. Conklin, N. Cornish, C. Cutler, K. Danzmann, R. Dolesi, L. Ferraioli, V. Ferroni, E. Fitzsimons, J. Gair, L. G. Bote, D. Giardini, F. Gibert, C. Grimani, H. Halloin, G. Heinzel, T. Hertog, M. Hewitson, K. Holley-Bockelmann, D. Hollington, M. Hueller, H. Inchauspe, P. Jetzer, N. Karnesis, C. Killow, A. Klein, B. Klipstein, N. Korsakova, S. L. Larson, J. Livas, I. Lloro, N. Man, D. Mance, J. Martino, I. Mateos, K. McKenzie, S. T. McWilliams, C. Miller, G. Mueller, G. Nardini, G. Nelemans, M. Nofrarias, A. Petiteau, P. Pivato, E. Plagnol, E. Porter, J. Reiche, D. Robertson, N. Robertson, E. Rossi, G. Rusano, B. Schutz, A. Sesana, D. Shoemaker, J. Slutsky, C. F. Sopuerta, T. Sumner, N. Tamanini, I. Thorpe, M. Troebs, M. Vallisneri, A. Vecchio, D. Vetrugno, S. Vitale, M. Volonteri, G. Wanner, H. Ward, P. Wass, W. Weber, J. Ziemer, and P. Zweifel, *Laser interferometer space antenna* (2017), [arXiv:1702.00786 \[astro-ph.IM\]](https://arxiv.org/abs/1702.00786).
- [2] S. Babak, J. Gair, A. Sesana, E. Barausse, C. F. Sopuerta, C. P. L. Berry, E. Berti, P. Amaro-Seoane, A. Petiteau, and A. Klein, *Phys. Rev. D* **95**, 103012 (2017).
- [3] P. A. Seoane *et al.* (LISA), *Living Rev. Rel.* **26**, 2 (2023), [arXiv:2203.06016 \[gr-qc\]](https://arxiv.org/abs/2203.06016).
- [4] P. Auclair *et al.* (LISA Cosmology Working Group), *Living Rev. Rel.* **26**, 5 (2023), [arXiv:2204.05434 \[astro-ph.CO\]](https://arxiv.org/abs/2204.05434).
- [5] J. Luo, L.-S. Chen, H.-Z. Duan, Y.-G. Gong, S. Hu, J. Ji, Q. Liu, J. Mei, V. Milyukov, M. Sazhin, C.-G. Shao, V. T. Toth, H.-B. Tu, Y. Wang, Y. Wang, H.-C. Yeh, M.-S. Zhan, Y. Zhang, V. Zharov, and Z.-B. Zhou, *Classical and Quantum Gravity* **33**, 035010 (2016).
- [6] J. Luo, Y.-Z. Bai, L. Cai, B. Cao, W.-M. Chen, Y. Chen, D.-C. Cheng, Y.-W. Ding, H.-Z. Duan, X. Gou, C.-Z. Gu, D.-F. Gu, Z.-Q. He, S. Hu, Y. Hu, X.-Q. Huang, Q. Jiang, Y.-Z. Jiang, H.-G. Li, H.-Y. Li, J. Li, M. Li, Z. Li, Z.-X. Li, Y.-R. Liang, F.-J. Liao, Y.-C. Liu, L. Liu, P.-B. Liu, X. Liu, Y. Liu, X.-F. Lu, Y. Luo, J. Mei, M. Ming, S.-B. Qu, D.-Y. Tan, M. Tang, L.-C. Tu, C.-R. Wang, F. Wang, G.-F. Wang, J. Wang, L. Wang, X. Wang, R. Wei, S.-C. Wu, C.-Y. Xiao, M.-Z. Xie, X.-S. Xu, L. Yang, M.-L. Yang, S.-Q. Yang, H.-C. Yeh, J.-B. Yu, L. Zhang, M.-H. Zhao, and Z.-B. Zhou, *Classical and Quantum Gravity* **37**, 185013 (2020).
- [7] J. Mei, Y.-Z. Bai, J. Bao, E. Barausse, L. Cai, E. Canuto, B. Cao, W.-M. Chen, Y. Chen, Y.-W. Ding, H.-Z. Duan, H. Fan, W.-F. Feng, H. Fu, Q. Gao, T. Gao, Y. Gong, X. Gou, C.-Z. Gu, D.-F. Gu, Z.-Q. He, M. Hendry, W. Hong, X.-C. Hu, Y.-M. Hu, Y. Hu, S.-J. Huang, X.-Q. Huang, Q. Jiang, Y.-Z. Jiang, Y. Jiang, Z. Jiang, H.-M. Jin, V. Korol, H.-Y. Li, M. Li, M. Li, P. Li, R. Li, Y. Li, Z. Li, Z. Li, Z.-X. Li, Y.-R. Liang, Z.-C. Liang, F.-J. Liao, Q. Liu, S. Liu, Y.-C. Liu, L. Liu, P.-B. Liu, X. Liu, Y. Liu, X.-F. Lu, Y. Lu, Z.-H. Lu, Y. Luo, Z.-C. Luo, V. Milyukov, M. Ming, X. Pi, C. Qin, S.-B. Qu, A. Sesana, C. Shao, C. Shi, W. Su, D.-Y. Tan, Y. Tan, Z. Tan, L.-C. Tu, B. Wang, C.-R. Wang, F. Wang, G.-F. Wang, H. Wang, J. Wang, L. Wang, P. Wang, X. Wang, Y. Wang, Y.-F. Wang, R. Wei, S.-C. Wu, C.-Y. Xiao, X.-S. Xu, C. Xue, F.-C. Yang, L. Yang, M.-L. Yang, S.-Q. Yang, B. Ye, H.-C. Yeh, S. Yu, D. Zhai, C. Zhang, H. Zhang, J.-d. Zhang, J. Zhang, L. Zhang, X. Zhang, X. Zhang, H. Zhou, M.-Y. Zhou, Z.-B. Zhou, D.-D. Zhu, T.-G. Zi, and

- J. Luo, *Progress of Theoretical and Experimental Physics* **2021**, 05A107 (2020), <https://academic.oup.com/ptep/article-pdf/2021/5/05A107/37953035/ptaa114.pdf>.
- [8] Y. Gong, J. Luo, and B. Wang, *Nature Astronomy* **5**, 881–889 (2021).
- [9] W.-R. Hu and Y.-L. Wu, *National Science Review* **4**, 685 (2017), <https://academic.oup.com/nsr/article-pdf/4/5/685/31566708/nwx116.pdf>.
- [10] W.-H. Ruan, Z.-K. Guo, R.-G. Cai, and Y.-Z. Zhang, *International Journal of Modern Physics A* **35**, 2050075 (2020), <https://doi.org/10.1142/S0217751X2050075X>.
- [11] B. Bonga, H. Yang, and S. A. Hughes, *Phys. Rev. Lett.* **123**, 101103 (2019), arXiv:1905.00030 [gr-qc].
- [12] B. Kocsis, N. Yunes, and A. Loeb, *Phys. Rev. D* **84**, 024032 (2011).
- [13] N. Yunes, B. Kocsis, A. Loeb, and Z. Haiman, *Phys. Rev. Lett.* **107**, 171103 (2011), arXiv:1103.4609 [astro-ph.CO].
- [14] L. Speri, A. Antonelli, L. Sberna, S. Babak, E. Barausse, J. R. Gair, and M. L. Katz, *Phys. Rev. X* **13**, 021035 (2023).
- [15] S. Chatterjee, S. Mondal, and P. Basu, *MNRAS* **526**, 5612 (2023), arXiv:2307.12144 [astro-ph.HE].
- [16] F. Duque, S. Kejriwal, L. Sberna, L. Speri, and J. Gair, Constraining accretion physics with gravitational waves from eccentric extreme-mass-ratio inspirals (2024), arXiv:2411.03436 [gr-qc].
- [17] J. Zhang and H. Yang, *Phys. Rev. D* **101**, 043020 (2020), arXiv:1907.13582 [gr-qc].
- [18] J. Zhang and H. Yang, *Phys. Rev. D* **99**, 064018 (2019), arXiv:1808.02905 [gr-qc].
- [19] R. Brito and S. Shah, *Phys. Rev. D* **108**, 084019 (2023), [Erratum: Phys.Rev.D 110, 109902 (2024)], arXiv:2307.16093 [gr-qc].
- [20] F. Duque, C. F. B. Macedo, R. Vicente, and V. Cardoso, *Phys. Rev. Lett.* **133**, 121404 (2024), arXiv:2312.06767 [gr-qc].
- [21] Z. Pan and H. Yang, *Phys. Rev. D* **103**, 103018 (2021), arXiv:2101.09146 [astro-ph.HE].
- [22] Y. Levin, *Mon. Not. Roy. Astron. Soc.* **374**, 515 (2007), arXiv:astro-ph/0603583.
- [23] Z. Pan, Z. Lyu, and H. Yang, *Phys. Rev. D* **104**, 063007 (2021), arXiv:2104.01208 [astro-ph.HE].
- [24] Z. Pan, Z. Lyu, and H. Yang, *Phys. Rev. D* **105**, 083005 (2022), arXiv:2112.10237 [astro-ph.HE].
- [25] L. Sun, X. Shu, and T. Wang, *Astrophys. J.* **768**, 167 (2013), arXiv:1304.3244 [astro-ph.GA].
- [26] G. Miniutti, R. D. Saxton, M. Giustini, K. D. Alexander, R. P. Fender, I. Heywood, I. Monageng, M. Coriat, A. K. Tzioumis, A. M. Read, C. Knigge, P. Gandhi, M. L. Pretorius, and B. Agís-González, *Nature (London)* **573**, 381 (2019), arXiv:1909.04693 [astro-ph.HE].
- [27] M. Giustini, G. Miniutti, and R. D. Saxton, *Astronomy&Astrophysics* **636**, L2 (2020), arXiv:2002.08967 [astro-ph.HE].
- [28] R. Arcodia, A. Merloni, K. Nandra, J. Buchner, M. Salvato, D. Pasham, R. Remillard, J. Comparat, G. Lamer, G. Ponti, A. Malyali, J. Wolf, Z. Arzoumanian, D. Bogensberger, D. A. H. Buckley, K. Gendreau, M. Gromadzki, E. Kara, M. Krumpe, C. Markwardt, M. E. Ramos-Ceja, A. Rau, M. Schramm, and A. Schwobe, *Nature (London)* **592**, 704 (2021), arXiv:2104.13388 [astro-ph.HE].
- [29] R. Arcodia, G. Miniutti, G. Ponti, J. Buchner, M. Giustini, A. Merloni, K. Nandra, F. Vincentelli, E. Kara, M. Salvato, and D. Pasham, *Astronomy&Astrophysics* **662**, A49 (2022), arXiv:2203.11939 [astro-ph.HE].
- [30] J. Chakraborty, E. Kara, M. Masterson, M. Giustini, G. Miniutti, and R. Saxton, *Astrophys.J.Lett.* **921**, L40 (2021), arXiv:2110.10786 [astro-ph.HE].
- [31] P. A. Evans, C. J. Nixon, S. Campana, P. Charalampopoulos, D. A. Perley, A. A. Breeveld, K. L. Page, S. R. Oates, R. A. J. Eyles-Ferris, D. B. Malesani, L. Izzo, M. R. Goad, P. T. O’Brien, J. P. Osborne, and B. Sbarufatti, *Nature Astronomy* **7**, 1368 (2023), arXiv:2309.02500 [astro-ph.HE].
- [32] S. Kejriwal, V. Witzany, M. Zajacek, D. R. Pasham, and A. J. K. Chua, *Mon. Not. Roy. Astron. Soc.* **532**, 2143 (2024), arXiv:2404.00941 [astro-ph.HE].
- [33] M. Guolo, D. R. Pasham, M. Zajaček, E. R. Coughlin, S. Gezari, P. Suková, T. Wevers, V. Witzany, F. Tombesi, S. van Velzen, K. D. Alexander, Y. Yao, R. Arcodia, V. Karas, J. C. A. Miller-Jones, R. Remillard, K. Gendreau, and E. C. Ferrara, *Nature Astronomy* **10**, 1038/s41550-023-02178-4 (2024), arXiv:2309.03011 [astro-ph.HE].
- [34] R. Arcodia, Z. Liu, A. Merloni, A. Malyali, A. Rau, J. Chakraborty, A. Goodwin, D. Buckley, J. Brink, M. Gromadzki, Z. Arzoumanian, J. Buchner, E. Kara, K. Nandra, G. Ponti, M. Salvato, G. Anderson, P. Baldini, I. Grotova, M. Krumpe, C. Maitra, J. C. A. Miller-Jones, and M. E. Ramos-Ceja, arXiv e-prints, arXiv:2401.17275 (2024), arXiv:2401.17275 [astro-ph.HE].
- [35] P. Peng, A. Franchini, M. Bonetti, A. Sesana, and X. Chen, The fate of EMRI-IMRI pairs in AGN accretion disks: long-term simulations (2024), arXiv:2411.16070 [astro-ph.HE].
- [36] H. Yang, B. Bonga, Z. Peng, and G. Li, *Phys. Rev. D* **100**, 124056 (2019), arXiv:1910.07337 [gr-qc].
- [37] M. Wang, Y. Ma, and Q. Wu, Accretion-modified stellar-mass black hole distribution and milli-Hz gravitational wave backgrounds from galaxy centre (2022), arXiv:2212.05724 [astro-ph.HE].
- [38] H. Tanaka, T. Takeuchi, and W. R. Ward, *The Astrophysical Journal* **565**, 1257 (2002).
- [39] H. Tanaka and W. R. Ward, *The Astrophysical Journal* **602**, 388 (2004).
- [40] E. Barausse, *Monthly Notices of the Royal Astronomical Society* **423**, 2533 (2012), <https://academic.oup.com/mnras/article-pdf/423/3/2533/7994573/mnras0423-2533.pdf>.
- [41] F. Shankar, D. H. Weinberg, and J. Miralda-Escudé, *The Astrophysical Journal* **690**, 20–41 (2008).
- [42] F. Shankar, *Classical and Quantum Gravity* **30**, 244001 (2013).
- [43] J. R. Gair, C. Tang, and M. Volonteri, *Phys. Rev. D* **81**, 104014 (2010).
- [44] Y. Yao, V. Ravi, S. Gezari, S. van Velzen, W. Lu, S. Schulze, J. J. Somalwar, S. R. Kulkarni, E. Hammerstein, M. Nicholl, M. J. Graham, D. A. Perley, S. B. Cenko, R. Stein, A. Ricarte, U. Chadayammuri, E. Quataert, E. C. Bellm, J. S. Bloom, R. Dekany, A. J. Drake, S. L. Groom, A. A. Mahabal, T. A. Prince, R. Riddle, B. Rusholme, Y. Sharma, J. Sollerman, and L. Yan, Tidal disruption event demographics with the zwicky transient facility: Volumetric rates, luminosity function, and implications for the local black hole mass function (2023), arXiv:2303.06523 [astro-ph.HE].
- [45] S. Babak, J. Gair, A. Sesana, E. Barausse, C. F. Sopuerta, C. P. L. Berry, E. Berti, P. Amaro-Seoane, A. Petiteau, and A. Klein, *Phys. Rev. D* **95**, 103012 (2017), arXiv:1703.09722 [gr-qc].
- [46] A. J. K. Chua, C. J. Moore, and J. R. Gair, *Phys. Rev. D* **96**, 044005 (2017).
- [47] M. L. Katz, A. J. K. Chua, L. Speri, N. Warburton, and S. A. Hughes, *Phys. Rev. D* **104**, 064047 (2021).
- [48] A. J. Chua, M. L. Katz, N. Warburton, and S. A. Hughes,

- Physical Review Letters **126**, 10.1103/physrevlett.126.051102 (2021).
- [49] R. Fujita and M. Shibata, Physical Review D **102**, 10.1103/physrevd.102.064005 (2020).
- [50] L. J. Rubbo, N. J. Cornish, and O. Poujade, Physical Review D **69**, 10.1103/physrevd.69.082003 (2004).
- [51] L. Barack and C. Cutler, Physical Review D **69**, 10.1103/physrevd.69.082005 (2004).
- [52] T. Robson, N. J. Cornish, and C. Liu, *Classical and Quantum Gravity* **36**, 105011 (2019).
- [53] S. Babak, M. Hewitson, and A. Petiteau, *Lisa sensitivity and snr calculations* (2021), arXiv:2108.01167 [astro-ph.IM].
- [54] J. M. Bardeen and J. A. Petterson, *Astroph.J.Lett.* **195**, L65 (1975).
- [55] P. Natarajan and J. E. Pringle, *Astroph.J.Lett.* **506**, L97 (1998), arXiv:astro-ph/9808187 [astro-ph].
- [56] G. Lodato and D. Gerosa, *MNRAS* **429**, L30 (2013), arXiv:1211.0284 [astro-ph.CO].
- [57] P. A. G. Scheuer and R. Feiler, *MNRAS* **282**, 291 (1996).
- [58] A. R. King, S. H. Lubow, G. I. Ogilvie, and J. E. Pringle, *MNRAS* **363**, 49 (2005), arXiv:astro-ph/0507098 [astro-ph].
- [59] D. Gerosa, G. Rosotti, and R. Barbieri, *MNRAS* **496**, 3060 (2020), arXiv:2004.02894 [astro-ph.GA].
- [60] J. Xian, F. Zhang, L. Dou, J. He, and X. Shu, *Astroph.J.Lett.* **921**, L32 (2021), arXiv:2110.10855 [astro-ph.HE].
- [61] I. Linial and B. D. Metzger, *Astrophys. J.* **957**, 34 (2023), arXiv:2303.16231 [astro-ph.HE].
- [62] A. Franchini, M. Bonetti, A. Lupi, G. Miniutti, E. Bortolas, M. Giustini, M. Dotti, A. Sesana, R. Arcodia, and T. Ryu, *Astronomy&Astrophysics* **675**, A100 (2023), arXiv:2304.00775 [astro-ph.HE].
- [63] H. Tagawa and Z. Haiman, arXiv e-prints , arXiv:2304.03670 (2023), arXiv:2304.03670 [astro-ph.HE].
- [64] I. Linial and B. D. Metzger, *Astrophys. J. Lett.* **963**, L1 (2024), arXiv:2311.16231 [astro-ph.HE].
- [65] C. Zhou, L. Huang, K. Guo, Y.-P. Li, and Z. Pan, *Phys. Rev. D* **109**, 103031 (2024), arXiv:2401.11190 [astro-ph.HE].
- [66] C. Zhou, B. Zhong, Y. Zeng, L. Huang, and Z. Pan, *Phys. Rev. D* **110**, 083019 (2024), arXiv:2405.06429 [astro-ph.HE].
- [67] C. Zhou, Y. Zeng, and Z. Pan, *Probing orbits of stellar mass objects deep in galactic nuclei with quasi-periodic eruptions – iii: Long term evolution* (2024), arXiv:2411.18046 [astro-ph.HE].
- [68] D. R. Pasham, E. R. Coughlin, M. Zajacek, I. Linial, P. Sukova, C. J. Nixon, A. Janiuk, M. Sniegowska, V. Witzany, V. Karas, M. Krumpe, D. Altamirano, T. Wevers, and R. Arcodia, arXiv e-prints , arXiv:2402.09690 (2024), arXiv:2402.09690 [astro-ph.HE].
- [69] J. Chakraborty, R. Arcodia, E. Kara, G. Miniutti, M. Giustini, A. J. Tetarenko, L. Rhodes, A. Franchini, M. Bonetti, K. B. Burdge, A. J. Goodwin, T. J. Maccarone, A. Merloni, G. Ponti, R. A. Remillard, and R. D. Saxton, arXiv e-prints , arXiv:2402.08722 (2024), arXiv:2402.08722 [astro-ph.HE].
- [70] I. Linial and B. D. Metzger, *Coupled disk-star evolution in galactic nuclei and the lifetimes of qpe sources* (2024), arXiv:2404.12421 [astro-ph.HE].
- [71] L. Arzamasskiy, Z. Zhu, and J. M. Stone, *MNRAS* **475**, 3201 (2018), arXiv:1710.11128 [astro-ph.EP].
- [72] Z. Zhu, *MNRAS* **483**, 4221 (2019), arXiv:1812.01262 [astro-ph.EP].
- [73] J. Davelaar and Z. Haiman, *Phys. Rev. Lett.* **128**, 191101 (2022), arXiv:2112.05829 [astro-ph.HE].
- [74] S. H. W. Leong, J. Janquart, A. K. Sharma, P. Martens, P. Ajith, and O. A. Hannuksela, *Constraining binary mergers in agn disks using the non-observation of lensed gravitational waves* (2024), arXiv:2408.13144 [astro-ph.HE].
- [75] Z. Pan and H. Yang, *The Astrophysical Journal* **901**, 163 (2020).
- [76] C. Liu, W.-H. Ruan, and Z.-K. Guo, *Phys. Rev. D* **107**, 064021 (2023).
- [77] J. Kormendy and L. C. Ho, *ARA&A* **51**, 511 (2013), arXiv:1304.7762 [astro-ph.CO].
- [78] R. I. Davies, J. Thomas, R. Genzel, F. Müller Sánchez, L. J. Tacconi, A. Sternberg, F. Eisenhauer, R. Abuter, R. Saglia, and R. Bender, *Astrophys. J.* **646**, 754 (2006), arXiv:astro-ph/0604125 [astro-ph].
- [79] C. A. Onken, M. Valluri, B. M. Peterson, R. W. Pogge, M. C. Bentz, L. Ferrarese, M. Vestergaard, D. M. Crenshaw, S. G. Sergeev, I. M. McHardy, D. Merritt, G. A. Bower, T. M. Heckman, and A. Wandel, *Astrophys. J.* **670**, 105 (2007), arXiv:0708.1196 [astro-ph].
- [80] H. Cho and J.-H. Woo, *Astrophys. J.* **969**, 93 (2024), arXiv:2405.09441 [astro-ph.GA].
- [81] E. Gallo, T. Treu, P. J. Marshall, J.-H. Woo, C. Leipski, and R. Antonucci, *Astrophys. J.* **714**, 25 (2010), arXiv:1002.3619 [astro-ph.HE].
- [82] T. T. Ananna, A. K. Weigel, B. Trakhtenbrot, M. J. Koss, C. M. Urry, C. Ricci, R. C. Hickox, E. Treister, F. E. Bauer, Y. Ueda, R. Mushotzky, F. Ricci, K. Oh, J. E. Mejia-Restrepo, J. D. Brok, D. Stern, M. C. Powell, T. Caglar, K. Ichikawa, O. I. Wong, F. A. Harrison, and K. Schawinski, *Astroph.J.S.* **261**, 9 (2022), arXiv:2201.05603 [astro-ph.HE].
- [83] F. Pacucci, M. Mezcuca, and J. A. Regan, *Astrophys. J.* **920**, 134 (2021), arXiv:2107.09069 [astro-ph.GA].
- [84] E. C. Moran, K. Shahinyan, H. R. Sugarman, D. O. Vélez, and M. Eracleous, *Astronomical Journal* **148**, 136 (2014), arXiv:1408.4451 [astro-ph.GA].
- [85] Y. Lu, T.-G. Wang, X.-B. Dong, and H.-Y. Zhou, *MNRAS* **404**, 1761 (2010), arXiv:1002.0632 [astro-ph.CO].
- [86] K. Oh, S. K. Yi, K. Schawinski, M. Koss, B. Trakhtenbrot, and K. Soto, *Astroph.J.S.* **219**, 1 (2015), arXiv:1504.07247 [astro-ph.GA].
- [87] Y. Shen, *Bulletin of the Astronomical Society of India* **41**, 61 (2013), arXiv:1302.2643 [astro-ph.CO].
- [88] B. M. Peterson, *Space Science Reviews* **183**, 253 (2014).
- [89] K. Gültekin, D. O. Richstone, K. Gebhardt, T. R. Lauer, S. Tremaine, M. C. Aller, R. Bender, A. Dressler, S. M. Faber, A. V. Filippenko, R. Green, L. C. Ho, J. Kormendy, J. Magorrian, J. Pinkney, and C. Siopis, *Astrophys. J.* **698**, 198 (2009), arXiv:0903.4897 [astro-ph.GA].
- [90] N. J. McConnell and C.-P. Ma, *Astrophys. J.* **764**, 184 (2013), arXiv:1211.2816 [astro-ph.CO].
- [91] L. C. Ho and M. Kim, *Astrophys. J.* **789**, 17 (2014), arXiv:1406.6137 [astro-ph.GA].
- [92] Gravity Collaboration, E. Sturm, J. Dexter, O. Pfuhl, M. R. Stock, R. I. Davies, D. Lutz, Y. Clénet, A. Eckart, F. Eisenhauer, R. Genzel, D. Gratadour, S. F. Hönig, M. Kishimoto, S. Lacour, F. Millour, H. Netzer, G. Perrin, B. M. Peterson, P. O. Petrucci, D. Rouan, I. Waisberg, J. Woillez, A. Amorim, W. Brandner, N. M. Förster Schreiber, P. J. V. Garcia, S. Gillessen, T. Ott, T. Paumard, K. Perraut, S. Scheithauer, C. Straubmeier, L. J. Tacconi, and F. Widmann, *Nature (London)* **563**, 657 (2018a), arXiv:1811.11195 [astro-ph.GA].
- [93] R. Abuter, F. Allouche, A. Amorim, C. Bailet, A. Berdeu, J. P. Berger, P. Berio, A. Bigioli, O. Boebion, M. L. Bolzer, H. Bonnet, G. Bourdarot, P. Bourget, W. Brandner, Y. Cao, R. Conzelmann, M. Comin, Y. Clénet, B. Courtney-Barrer, R. Davies, D. Defrère, A. Delboulbé, F. Delplancke-Ströbele,

- R. Dembet, J. Dexter, P. T. de Zeeuw, A. Drescher, A. Eckart, C. Édouard, F. Eisenhauer, M. Fabricius, H. Feuchtgruber, G. Finger, N. M. Förster Schreiber, P. Garcia, R. Garcia Lopez, F. Gao, E. Gendron, R. Genzel, J. P. Gil, S. Gillessen, T. Gomes, F. Gonté, C. Gouvret, P. Guajardo, S. Guieu, W. Hackenberg, N. Haddad, M. Hartl, X. Haubois, F. Haußmann, G. Heißel, T. Henning, S. Hippler, S. F. Hönig, M. Horrobin, N. Hubin, E. Jacqmart, L. Jocou, A. Kaufer, P. Kervella, J. Kolb, H. Korhonen, S. Lacour, S. Lagarde, O. Lai, V. Lapeyrière, R. Laugier, J. B. Le Bouquin, J. Lefley, P. Léna, S. Lewis, D. Liu, B. Lopez, D. Lutz, Y. Magnard, F. Mang, A. Marcotto, D. Maurel, A. Mérand, F. Millour, N. More, H. Netzer, H. Nowacki, M. Nowak, S. Oberti, T. Ott, L. Pallanca, T. Paumard, K. Perraut, G. Perrin, R. Petrov, O. Pfuhl, N. Poiré, S. Rabien, C. Rau, M. Riquelme, S. Robbe-Dubois, S. Rochat, M. Salman, J. Sanchez-Bermudez, D. J. D. Santos, S. Scheithauer, M. Schöller, J. Schubert, N. Schuhler, J. Shanguan, P. Shchekaturov, T. T. Shimizu, A. Sevin, F. Soulez, A. Spang, E. Stadler, A. Sternberg, C. Straubmeier, E. Sturm, C. Sykes, L. J. Tacconi, K. R. W. Tristram, F. Vincent, S. von Fellenberg, S. Uysal, F. Widmann, E. Wieprecht, E. Wiezorek, J. Woillez, and G. Zins, *Nature (London)* **627**, 281 (2024), [arXiv:2401.14567 \[astro-ph.GA\]](#).
- [94] Y. Tanaka, K. Nandra, A. C. Fabian, H. Inoue, C. Otani, T. Dotani, K. Hayashida, K. Iwasawa, T. Kii, H. Kunieda, F. Makino, and M. Matsuoka, *Nature (London)* **375**, 659 (1995).
- [95] J. García, T. Dauser, A. Lohfink, T. R. Kallman, J. F. Steiner, J. E. McClintock, L. Brenneman, J. Wilms, W. Eikmann, C. S. Reynolds, and F. Tombesi, *Astrophys. J.* **782**, 76 (2014), [arXiv:1312.3231 \[astro-ph.HE\]](#).
- [96] C. S. Reynolds, *Annual Review of Astronomy and Astrophysics* **59**, 117–154 (2021).
- [97] S. G. H. Waddell and L. C. Gallo, *MNRAS* **498**, 5207 (2020), [arXiv:2009.04378 \[astro-ph.HE\]](#).
- [98] R. V. Vasudevan and A. C. Fabian, *MNRAS* **392**, 1124 (2009), [arXiv:0810.3777 \[astro-ph\]](#).
- [99] N. Cappelluti, M. Brusa, G. Hasinger, A. Comastri, G. Zamorani, A. Finoguenov, R. Gilli, S. Puccetti, T. Miyaji, M. Salvato, C. Vignali, T. Aldcroft, H. Böhringer, H. Brunner, F. Civano, M. Elvis, F. Fiore, A. Fruscione, R. E. Griffiths, L. Guzzo, A. Iovino, A. M. Koekemoer, V. Mainieri, N. Z. Scoville, P. Shopbell, J. Silverman, and C. M. Urry, *Astronomy&Astrophysics* **497**, 635 (2009), [arXiv:0901.2347 \[astro-ph.HE\]](#).
- [100] M. J. Koss, C. Ricci, B. Trakhtenbrot, K. Oh, J. S. den Brok, J. E. Mejía-Restrepo, D. Stern, G. C. Privon, E. Treister, M. C. Powell, R. Mushotzky, F. E. Bauer, T. T. Ananna, M. Baloković, R. E. Bär, G. Becker, P. Bessiere, L. Burtscher, T. Caglar, E. Congiu, P. Evans, F. Harrison, M. Heida, K. Ichikawa, N. Kamraj, I. Lamperti, F. Pacucci, F. Ricci, R. Riffel, A. F. Rojas, K. Schawinski, M. J. Temple, C. M. Urry, S. Veilleux, and J. Williams, *Astroph.J.S.* **261**, 2 (2022), [arXiv:2207.12432 \[astro-ph.GA\]](#).
- [101] S. N. Zhang, M. Feroci, A. Santangelo, Y. W. Dong, H. Feng, F. J. Lu, K. Nandra, Z. S. Wang, S. Zhang, E. Bozzo, S. Brandt, A. De Rosa, L. J. Gou, M. Hernanz, M. van der Klis, X. D. Li, Y. Liu, P. Orleanski, G. Pareschi, M. Pohl, J. Poutanen, J. L. Qu, S. Schanne, L. Stella, P. Uttley, A. Watts, R. X. Xu, W. F. Yu, J. J. M. in 't Zand, S. Zane, L. Alvarez, L. Amati, L. Baldini, C. Bambi, S. Basso, Bhattacharyya S., R. , Bellazzini, T. Belloni, P. Bellutti, S. Bianchi, A. Brez, M. Bursa, V. Burwitz, C. Budtz-Jørgensen, I. Caiazzo, R. Campana, X. Cao, P. Casella, C. Y. Chen, L. Chen, T. Chen, Y. Chen, Y. Chen, Y. P. Chen, M. Civitani, F. Coti Zelati, W. Cui, W. W. Cui, Z. G. Dai, E. Del Monte, D. de Martino, S. Di Cosimo, S. Diebold, M. Dovciak, I. Donnarumma, V. Doroshenko, P. Esposito, Y. Evangelista, Y. Favre, P. Friedrich, F. Fuschino, J. L. Galvez, Z. L. Gao, M. Y. Ge, O. Gevin, D. Goetz, D. W. Han, J. Heyl, J. Horak, W. Hu, F. Huang, Q. S. Huang, R. Hudec, D. Huppenkothen, G. L. Israel, A. Ingram, V. Karas, D. Karelín, P. A. Jenke, L. Ji, S. Korpela, D. Kunneriath, C. Labanti, G. Li, X. Li, Z. S. Li, E. W. Liang, O. Limousin, L. Lin, Z. X. Ling, H. B. Liu, H. W. Liu, Z. Liu, B. Lu, N. Lund, D. Lai, B. Luo, T. Luo, B. Ma, S. Mahmoodifar, M. Marisaldi, A. Martindale, N. Meidinger, Y. Men, M. Michalska, R. Mignani, M. Minuti, S. Motta, F. Muleri, J. Neilsen, M. Orlandini, A. T. Pan, A. Patruno, E. Perinati, A. Picciotto, C. Piemonte, M. Pinchera, Rachevski A., M. Rapisarda, N. Rea, E. M. R. Rossi, A. Rubini, G. Sala, X. W. Shu, C. Sgro, Z. X. Shen, P. Soffitta, L. Song, G. Spandre, G. Stratta, T. E. Strohmayer, L. Sun, J. Svoboda, G. Tagliaferrri, G. Tenzer, T. Hong, R. Taverna, G. Torok, R. Turolla, S. Vacchi, J. Wang, D. Walton, K. Wang, J. F. Wang, R. J. Wang, Y. F. Wang, S. S. Weng, J. Wilms, B. Winter, X. Wu, X. F. Wu, S. L. Xiong, Y. P. Xu, Y. Q. Xue, Z. Yan, S. Yang, X. Yang, Y. J. Yang, F. Yuan, W. M. Yuan, Y. F. Yuan, G. Zampa, N. Zampa, A. Zdziarski, C. Zhang, C. L. Zhang, L. Zhang, X. Zhang, Z. Zhang, W. D. Zhang, S. J. Zheng, P. Zhou, and Zhou X. L., in *Space Telescopes and Instrumentation 2016: Ultraviolet to Gamma Ray*, Society of Photo-Optical Instrumentation Engineers (SPIE) Conference Series, Vol. 9905, edited by J.-W. A. den Herder, T. Takahashi, and M. Bautz (2016) p. 99051Q, [arXiv:1607.08823 \[astro-ph.IM\]](#).
- [102] K. Nandra, D. Barret, X. Barcons, A. Fabian, J.-W. den Herder, L. Piro, M. Watson, C. Adami, J. Aird, J. M. Afonso, D. Alexander, C. Argiroffi, L. Amati, M. Arnaud, J.-L. Atteia, M. Audard, C. Badenes, J. Ballet, L. Ballo, A. Bamba, A. Bhardwaj, E. Stefano Battistelli, W. Becker, M. De Becker, E. Behar, S. Bianchi, V. Biffi, L. Bîrzan, F. Bocchino, S. Bogdanov, L. Boirin, T. Boller, S. Borgani, K. Borm, N. Bouché, H. Bourdin, R. Bower, V. Braito, E. Branchini, G. Branduardi-Raymont, J. Bregman, L. Brenneman, M. Brightman, M. Brüggen, J. Buchner, E. Bulbul, M. Brusa, M. Bursa, A. Caccianiga, E. Cackett, S. Campana, N. Cappelluti, M. Cappi, F. Carrera, M. Ceballos, F. Christensen, Y.-H. Chu, E. Churazov, N. Clerc, S. Corbel, A. Corral, A. Comastri, E. Costantini, J. Croston, M. Dadina, A. D’Ai, A. Decourchelle, R. Della Ceca, K. Dennerl, K. Dolag, C. Done, M. Dovciak, J. Drake, D. Eckert, A. Edge, S. Etori, Y. Ezoe, E. Feigelson, R. Fender, C. Feruglio, A. Finoguenov, F. Fiore, M. Galeazzi, S. Gallagher, P. Gandhi, M. Gaspari, F. Gastaldello, A. Georgakakis, I. Georgantopoulos, M. Gilfanov, M. Gitti, R. Gladstone, R. Goosmann, E. Gosset, N. Grosso, M. Guedel, M. Guerrero, F. Haberl, M. Hardcastle, S. Heinz, A. Alonso Herrero, A. Hervé, M. Holmstrom, K. Iwasawa, P. Jonker, J. Kaasstra, E. Kara, V. Karas, J. Kastner, A. King, D. Kosenko, D. Koutroumpa, R. Kraft, I. Kreykenbohm, R. Lalleman, G. Lanzuisi, J. Lee, M. Lemoine-Goumard, A. Lobban, G. Lodato, L. Lovisari, S. Lotti, I. McCarthy, B. McNamara, A. Maggio, R. Maiolino, B. De Marco, D. de Martino, S. Mateos, G. Matt, B. Maughan, P. Mazzotta, M. Mendez, A. Merloni, G. Micela, M. Miceli, R. Mignani, J. Miller, G. Miniutti, S. Molendi, R. Montez, A. Moretti, C. Motch, Y. Nazé, J. Nevalainen, F. Nicastro, P. Nulsen, T. Ohashi, P. O’Brien, J. Osborne, L. Oskinova, F. Pacaud, F. Paerels, M. Page, I. Papadakis, G. Pareschi, R. Petre, P.-O. Petrucci, E. Piconcelli,

- I. Pillitteri, C. Pinto, J. de Plaa, E. Pointecouteau, T. Ponman, G. Ponti, D. Porquet, K. Pounds, G. Pratt, P. Predohl, D. Proga, D. Psaltis, D. Rafferty, M. Ramos-Ceja, P. Ranalli, E. Rasia, A. Rau, G. Rauw, N. Rea, A. Read, J. Reeves, T. Reiprich, M. Renaud, C. Reynolds, G. Risaliti, J. Rodriguez, P. Rodriguez Hidalgo, M. Roncarelli, D. Rosario, M. Rossetti, A. Rozanska, E. Rovilos, R. Salvaterra, M. Salvato, T. Di Salvo, J. Sanders, J. Sanz-Forcada, K. Schawinski, J. Schaye, A. Schwobe, S. Sciortino, P. Severgnini, F. Shankar, D. Sijacki, S. Sim, C. Schmid, R. Smith, A. Steiner, B. Stelzer, G. Stewart, T. Strohmayer, L. Strüder, M. Sun, Y. Takei, V. Tatischeff, A. Tiengo, F. Tombesi, G. Trinchieri, T. G. Tsuru, A. Ud-Doula, E. Ursino, L. Valencic, E. Vanzella, S. Vaughan, C. Vignali, J. Vink, F. Vito, M. Volonteri, D. Wang, N. Webb, R. Willingale, J. Wilms, M. Wise, D. Worrall, A. Young, L. Zampieri, J. In't Zand, S. Zane, A. Zezas, Y. Zhang, and I. Zhuravleva, *arXiv e-prints*, [arXiv:1306.2307](https://arxiv.org/abs/1306.2307) (2013), [arXiv:1306.2307](https://arxiv.org/abs/1306.2307) [astro-ph.HE].
- [103] C. S. Reynolds, *Space Science Reviews* **183**, 277–294 (2013).
- [104] NED, *The nasa/ipac extragalactic database (ned)* (2024).
- [105] R. D. Blandford and R. L. Znajek, *Monthly Notices of the Royal Astronomical Society* **179**, 433 (1977), <https://academic.oup.com/mnras/article-pdf/179/3/433/9333653/mnras179-0433.pdf>.
- [106] A. Tchekhovskoy, R. Narayan, and J. C. McKinney, *Monthly Notices of the Royal Astronomical Society: Letters* **418**, L79 (2011), <https://academic.oup.com/mnrasl/article-pdf/418/1/L79/56939896/mnrasl.418.1.L79.pdf>.
- [107] R. D. Blandford and D. G. Payne, *MNRAS* **199**, 883 (1982).
- [108] D. L. Meier, D. G. Payne, and K. R. Lind, in *Extragalactic Radio Sources*, IAU Symposium, Vol. 175, edited by R. D. Ekers, C. Fanti, and L. Padrielli (1996) p. 433.
- [109] J. M. Bardeen and J. A. Petterson, *Astrophys. J. Lett.* **195**, L65 (1975).
- [110] F. D. Ryan, *Phys. Rev. D* **52**, R3159 (1995).
- [111] S. A. Hughes, *Phys. Rev. D* **61**, 084004 (2000).
- [112] K. Glampedakis, S. A. Hughes, and D. Kennefick, *Phys. Rev. D* **66**, 064005 (2002).
- [113] J. R. Gair and K. Glampedakis, *Phys. Rev. D* **73**, 064037 (2006).
- [114] T. Hovatta, E. Valtaoja, M. Tornikoski, and A. Lähteenmäki, *Astronomy&Astrophysics* **494**, 527–537 (2008).
- [115] A. B. Pushkarev, Y. Y. Kovalev, M. L. Lister, and T. Savolainen, *Astronomy&Astrophysics* **507**, L33–L36 (2009).
- [116] M. L. Lister, M. H. Cohen, D. C. Homan, M. Kadler, K. I. Kellermann, Y. Y. Kovalev, E. Ros, T. Savolainen, and J. A. Zensus, *The Astronomical Journal* **138**, 1874 (2009).
- [117] M. L. Lister, M. F. Aller, H. D. Aller, D. C. Homan, K. I. Kellermann, Y. Y. Kovalev, A. B. Pushkarev, J. L. Richards, E. Ros, and T. Savolainen, *The Astronomical Journal* **152**, 12 (2016).
- [118] A. B. Pushkarev, Y. Y. Kovalev, M. L. Lister, and T. Savolainen, *Monthly Notices of the Royal Astronomical Society* **468**, 4992 (2017), <https://academic.oup.com/mnras/article-pdf/468/4/4992/17155561/stx854.pdf>.
- [119] M. L. Lister, M. F. Aller, H. D. Aller, M. A. Hodge, D. C. Homan, Y. Y. Kovalev, A. B. Pushkarev, and T. Savolainen, *The Astrophysical Journal Supplement Series* **234**, 12 (2018).
- [120] M. L. Lister, D. C. Homan, T. Hovatta, K. I. Kellermann, S. Kiehlmann, Y. Y. Kovalev, W. Max-Moerbeck, A. B. Pushkarev, A. C. S. Readhead, E. Ros, and T. Savolainen, *The Astrophysical Journal* **874**, 43 (2019).
- [121] M. L. Lister, D. C. Homan, K. I. Kellermann, Y. Y. Kovalev, A. B. Pushkarev, E. Ros, and T. Savolainen, *The Astrophysical Journal* **923**, 30 (2021).
- [122] M. Katz, CChapmanbird, L. Speri, N. Karnesis, and N. Korsakova, [mikekatz04/lisaanalysisistools: First main release](https://arxiv.org/abs/2401.11111). (2024).
- [123] B. P. Abbott *et al.* (LIGO Scientific, Virgo, 1M2H, Dark Energy Camera GW-E, DES, DLT40, Las Cumbres Observatory, VINROUGE, MASTER), *Nature* **551**, 85 (2017), [arXiv:1710.05835](https://arxiv.org/abs/1710.05835) [astro-ph.CO].
- [124] A. G. Riess, S. Casertano, W. Yuan, J. B. Bowers, L. Macri, J. C. Zinn, and D. Scolnic, *The Astrophysical Journal Letters* **908**, L6 (2021).
- [125] D. Laghi, N. Tamanini, W. Del Pozzo, A. Sesana, J. Gair, S. Babak, and D. Izquierdo-Villalba, *Mon. Not. Roy. Astron. Soc.* **508**, 4512 (2021), [arXiv:2102.01708](https://arxiv.org/abs/2102.01708) [astro-ph.CO].
- [126] W. Del Pozzo and D. Laghi, [mikekatz04/lisaanalysisistools: First main release](https://arxiv.org/abs/2009.01111). (2020).
- [127] N. Tamanini, C. Caprini, E. Barausse, A. Sesana, A. Klein, and A. Petiteau, *Journal of Cosmology and Astroparticle Physics* **2016** (04), 002.
- [128] P. A. R. Ade *et al.* (Planck), *Astron. Astrophys.* **594**, A13 (2016), [arXiv:1502.01589](https://arxiv.org/abs/1502.01589) [astro-ph.CO].
- [129] N. Aghanim *et al.* (Planck), *Astron. Astrophys.* **641**, A6 (2020), [Erratum: *Astron. Astrophys.* 652, C4 (2021)], [arXiv:1807.06209](https://arxiv.org/abs/1807.06209) [astro-ph.CO].
- [130] A. G. Riess *et al.*, *Astrophys. J. Lett.* **934**, L7 (2022), [arXiv:2112.04510](https://arxiv.org/abs/2112.04510) [astro-ph.CO].
- [131] S. Mukherjee, G. Lavaux, F. R. Bouchet, J. Jasche, B. D. Wandelt, S. M. Nissanke, F. Leclercq, and K. Hotokezaka, *Astron. Astrophys.* **646**, A65 (2021), [arXiv:1909.08627](https://arxiv.org/abs/1909.08627) [astro-ph.CO].
- [132] T. L. S. Collaboration and the Virgo Collaboration, *The Astrophysical Journal* **909**, 218 (2021).
- [133] S. Capozziello and M. Francaviglia, *General Relativity and Gravitation* **40**, 357–420 (2007).
- [134] S. Capozziello and M. De Laurentis, *Physics Reports* **509**, 167 (2011).
- [135] Y.-F. Cai, S. Capozziello, M. D. Laurentis, and E. N. Saridakis, *Reports on Progress in Physics* **79**, 106901 (2016).
- [136] R. C. Nunes, A. Bonilla, S. Pan, and E. N. Saridakis, *The European Physical Journal C* **77**, 10.1140/epjc/s10052-017-4798-5 (2017).
- [137] S. Nojiri, S. Odintsov, and V. Oikonomou, *Physics Reports* **692**, 1 (2017), modified Gravity Theories on a Nutshell: Inflation, Bounce and Late-time Evolution.
- [138] I. Quiros, *International Journal of Modern Physics D* **28**, 1930012 (2019), <https://doi.org/10.1142/S021827181930012X>.
- [139] M. Raveri, *Phys. Rev. D* **101**, 083524 (2020).
- [140] T. Clifton, P. G. Ferreira, A. Padilla, and C. Skordis, *Physics Reports* **513**, 1 (2012), modified Gravity and Cosmology.
- [141] J. Weller and A. Albrecht, *Phys. Rev. D* **65**, 103512 (2002).
- [142] R. Fardon, A. E. Nelson, and N. Weiner, *Journal of Cosmology and Astroparticle Physics* **2004** (10), 005.
- [143] T. Karwal and M. Kamionkowski, *Phys. Rev. D* **94**, 103523 (2016).
- [144] G.-B. Zhao *et al.*, *Nature Astron.* **1**, 627 (2017), [arXiv:1701.08165](https://arxiv.org/abs/1701.08165) [astro-ph.CO].
- [145] A. Bonilla, S. Kumar, and R. C. Nunes, *Eur. Phys. J. C* **81**, 127 (2021), [arXiv:2011.07140](https://arxiv.org/abs/2011.07140) [astro-ph.CO].
- [146] B. S. Haridasu, V. V. Luković, M. Moresco, and N. Vittorio, *Journal of Cosmology and Astroparticle Physics* **2018** (10), 015.

- [147] A. Gómez-Valent and L. Amendola, *Journal of Cosmology and Astroparticle Physics* **2018** (04), 051.
- [148] H. Yu, B. Ratra, and F.-Y. Wang, *The Astrophysical Journal* **856**, 3 (2018).
- [149] C. R. Burns, E. Parent, M. M. Phillips, M. Stritzinger, K. Krisciunas, N. B. Suntzeff, E. Y. Hsiao, C. Contreras, J. Anais, L. Boldt, L. Busta, A. Campillay, S. Castellón, G. Folatelli, W. L. Freedman, C. González, M. Hamuy, P. Heoflich, W. Krzeminski, B. F. Madore, N. Morrell, S. E. Persson, M. Roth, F. Salgado, J. Serón, and S. Torres, *The Astrophysical Journal* **869**, 56 (2018).
- [150] G. Efstathiou, A Lockdown Perspective on the Hubble Tension (with comments from the SHOES team) (2020), [arXiv:2007.10716](https://arxiv.org/abs/2007.10716) [astro-ph.CO].
- [151] T. A. Thompson, E. Quataert, and N. Murray, *Astrophys. J.* **630**, 167 (2005), [arXiv:astro-ph/0503027](https://arxiv.org/abs/astro-ph/0503027).